The Henryk Niewodniczański
Institute of Nuclear Physics
Kraków, Poland

INP

Report No 1732/PL

STUDIES OF REACTION MECHANISM IN $^{12}C + ^{12}C$ SYSTEMS AT INTERMEDIATE ENERGY OF 28.7 MeV/N

Andrzej Magiera

Address: 29 - 29

Main site:
ul. Radzikowskiego 152,
31-342 Kraków, Poland
e-mail: dyrektor@bron.ifj.edu.pl

High Energy Department:
ul. Kawiory 26 A,
30-055 Kraków, Poland
e-mail: hepsec@chopin.ifj.edu.pl

REPORT No 1732/PL

Studies of reaction mechanism in $^{12}C+^{12}C$ system at intermediate energy of 28.7 MeV/nucleon

Andrzej Magiera

Institute of Physics, Jagellonian University

Cracow 1996

Wydano nakładem
Instytutu Fizyki
Uniwersytetu Jagiellońskiego
w Krakowie

s.c. tel. (012) 370222 w. 323

Contents

1. Introduction

In the investigations of nucleus–nucleus collisions at intermediate energies large effort is concentrated on studies of the reaction mechanism leading to many body final state. It is expected that in the beam energy range from 20 to 100 MeV/nucleon a new phenomena may occur. This energy range is transitional between low energy regime where mean field determines the interaction process and high energy region where collisions of individual nucleons dominate. In intermediate energy region a strong competition between low and high energy reaction mechanisms should appear. Therefore besides the reaction mechanisms (compound nucleus and direct reactions) dominating at low energies, other models responsible for production of many particles in exit channel are regarded. Two basic, extreme models of reactions leading to multiparticle final state are considered: the first one similar to that observed at low energies – sequential binary decay, the second one predicted for large energies – simultaneous disassembly (prompt fragmentation). The analysis of the reaction mechanism may provide informations about properties and decay modes of highly excited nuclei. Very intensive searching for prompt fragmentation process is related to possibility of observation of the liquid–gas phase transition in the nuclear matter.

The goal of this work was to investigate the interaction between light heavy nuclei by studying various outgoing channels at intermediate energies. A special attention was devoted to the processes leading to a few particles in the exit channel. Such processes dominate the reaction cross section. The interpretation of results of analysis for a few body final states is difficult and many controversies exist about the reaction mechanism leading to many body final states.

A classification of various reaction mechanisms proposed for intermediate energy region as well as review of experimental data and different theories and models are presented in ref. 1. In spite of numerous experimental investigations[2–49] and variety of proposed models[50–62] for the reaction mechanism the situation is still unclear. This is caused by the fact that the performed experiments are not able to distinguish well between different processes such as sequential fragmentation processes and prompt fragmentation. Moreover the models of sequential and prompt fragmentation predict very similar results for different experimental observables, since their general features are governed mainly by the available phase space.

The experimental investigations cover inclusive and coincidence measurements. They were performed usually for light beam and heavy target or both heavy beam and target nuclei. In such a case the analysis of the experimental data is complicated due to large number of nucleons in the investigated system. For heavy and especially for very asymmetric systems the high probability of the target excitation (due to the large density of states) strongly influences the projectile fragmentation process. Only a few measurements were done for both light beam and target nuclei combinations[4,38,39,48,49]. In the inclusive experiments the energy and angular distributions of various ejectiles were measured normally with their mass and charge separation. The coincidence experiments were usually performed with multidetector arrays which allow the detection of many outgoing particles in coincidence, however only the charge separation of heavy ejectiles is possible. This enables the reconstruction of properties of decaying system but some corrections are necessary to take into

account finite detection threshold and emission of neutrons not detected by such systems. The large detection threshold causes that only fragments emitted from projectile like particles are detected, while those from target like nuclei fall below detection threshold. In some cases single detectors allowing also mass separation were included to such detection systems.

The inclusive data were analysed in the frames of different models. Some of them based on simple parameterization[34,39,48,63,64] or moving source approximation[7,30,47] allowing general overview of the experimental data only. More advanced models like the Cole model[65,66] including evaporation of particles after excitation of interacting nuclei, elastic break-up and transfer[67] or an extended Serber model[68] may account for particular features of the observed data. The measured observables (mass and charge distributions, fragment energy distributions, angular distributions) are not sufficient to disentangle prompt and sequential fragmentation. Thus the exclusive measurements are necessary in order to shed more light on the reaction mechanism at intermediate energies. From the coincidence measurements some quantities may be obtained directly. They include measurements of: projectile like fragment velocity, excitation energy of the source of observed particles, the energy sharing between projectile and target like fragments. This is however done under assumption of observation of all final state fragments, what was not fulfilled in any of performed experiments. In order to find more clear experimental signature distinguishing prompt and sequential fragmentation it was proposed[69] to look for some kinematic difference between these two processes. Some of the data for a specific outgoing channels were analysed using this method[13,33,36,70] leading to the conclusion that experimental data better agree with the sequential fragmentation mechanism[13,36], however observation of prompt fragmentation cannot be excluded[33,70]. Following the idea of ref. 69 the influence of the Coulomb interaction on trajectories of fragments emitted from a hot nuclear system was investigated[71]. It was found that pronounced differences in angular distribution of the velocity vectors of fragments appear for prompt and sequential fragmentation. The comparison of these prediction with the experimental data[72] may suggest the observation of prompt fragmentation. Very promising are the investigations of excitation functions of various observables, performed in order to find the dramatic changes in their behaviour with increasing beam energy indicating appearance of new reaction mechanism. Unfortunately such studies led to completely inconsistent conclusions. Only sequential processes are observed in the range of incident energy form 25 to 95 MeV/nucleon for various systems[2,4,10,13,16,73], or the smooth evolution to prompt fragmentation is noticed[37,47], while some dramatic changes are found for Dalitz plot at 52 MeV/nucleon[3], for charge distributions for central collisions at 35 MeV/nucleon[19] and for mean emission lifetimes at 55 MeV/nucleon[14]. Most of the interpretations of coincidence results base on the Monte-Carlo simulations performed assuming some angular and excitation energy distributions of the primary fragments and requesting statistical equilibrium in each stage before particle emission. Most frequently it is shown that sequential decay may account for observed coincidences (only qualitative comparison is done), however some authors claim the observation of nonsequential processes[8,9,27,40,44]. It should be pointed out that even such simple analysis leads to contradictory conclusions (e.g. complete isotropy of the decay in c.m. system of decaying nucleus[32] in contrary to the strong alignment of the decaying nuclei[15]).

In the present work measurements were performed for system of light heavy ions $^{12}C+^{12}C$ at incident energy of 28.7 MeV/nucleon. The beam energy is above the energy where the appearance of the processes different from that at low energies is expected. The choice of entrance channel nuclei in the present experiment allows for considerable simplification of the analysis. Firstly the study of the interaction of light heavy ions limits the number of possible partitions in the observed final state. Secondly the identity of interacting nuclei in the entrance channel and therefore fore–aft symmetry in the center of mass frame puts very stringent constraints on the data. In such a case the identical processes of production and fragmentation of projectile and target like nuclei appear. Therefore the reactions with many body exit channel might be measured by the observation of fragmentation products of projectile like nuclei and owing to the symmetry by the observation of associated target like nuclei. In the present case the projectile and target like nuclei could not be distinguished by their masses. They differ only by their velocities in the laboratory reference frame. Projectile like nuclei i.e. fragments of the projectile will have large velocities in the laboratory system, while target like nuclei rather small ones. The additional experimental advantage of using light nuclei in entrance channel is that the reaction products are also light, what makes possible their detection with low energy threshold, with good mass and charge separation of ejectiles and good energy resolution. The inclusive measurements of the energy spectra and angular distributions for various ejectiles (from ^{4}He up to ^{15}N) as well as coincidence measurements in different angular configurations were performed. The differential inclusive and coincidence cross sections were extracted. That leads to large set of the experimental data containing transitions leading to discrete bound or unbound states of ejectiles, the continuous spectra that correspond to the excitation of highly excited states of ejectiles or to many body reactions, and the correlation of two particles emitted in many body processes. The experimental data were analysed by means of various methods. The coincidence data were analysed basing on the kinematical considerations. That allowed to obtain model independent information about the reaction mechanism leading to many particles in the exit channel. The inelastic excitation[74] and transfer reactions to discrete states[75] were analysed within the standard DWBA. The inelastic excitations to higher excited states were calculated[76,77] with Multistep Direct Reaction (MSDR) model, the one nucleon transfer reactions leading to unbound states were analysed[77] using DWBA and strength functions calculated microscopically. The compound nucleus reactions were analysed with the standard Hauser-Feshbach statistical model. The phenomenological approach was applied in the analysis of sequential decay processes initiated by the inelastic excitation and transfer reactions.

The experimental procedure will be presented in chapter 2 together with the discussion of characteristic features of the experimental data. In chapter 3 results of the analysis in the frame of compound nucleus and direct (MSDR and DWBA) reaction models are given. The model independent qualitative discussion of the coincidence data based on the kinematical signatures of the sequential fragmentation is presented in chapter 4. The model used for the analysis of the sequential processes initiated by direct reactions is presented in chapter 5. The results of the phenomenological analysis of sequential fragmentation processes are compared with experimental data in chapter 6 for inclusive and coincidence distributions. In chapter 7 the contribution of various reaction mechanisms is discussed and final conclusions are presented.

2. Experimental procedure and results

2.1. Experimental set–up and procedure

The experiments were performed using ^{12}C ion beam of 344.5 MeV energy from the JULIC cyclotron of the Forschungszentrum Jülich. The experiments included the inclusive energy spectra and coincidence measurements. The beam was focused on ^{12}C target of 1.1 mg/cm^2 thickness. The detection system contained three counter telescopes consisted of 50 μm, 400 μm, 2 mm and 6 mm thick Si surface barrier detectors. The solid angle covered by the detectors was 0.04 msr in inclusive experiments in order to have a good angular resolution. In case of coincidence measurements solid angle was 0.2 msr in order to increase the detection efficiency and true to random coincidences ratio. The detectors were cooled down to the temperature of –20°C. This detection system allowed to separate the reaction products from ^4He up to ^{15}N according to their mass and charge in the energy range starting from about 3–4 MeV/nucleon threshold. The energy resolution was 0.2%. The time differences of the pulses from the telescope pairs in coincidence were measured in the exclusive experiments with the resolution of about 1 ns. This allowed the subtraction of the random coincidence events in the further off-line analysis.

The absolute calibration of the energy was performed by proper adjustment of the relative amplification of electronics and by comparing the known energies of different outgoing particles with the position of the corresponding peaks observed experimentally. The achieved accuracy of the absolute energy scale was about 0.8%.

For separation of different ejectiles, the identification parameter was calculated according to formula[78]:

$$\mathbf{p} = (\Delta E + E)^b - E^b$$

using pulses ΔE and E from the transmission and stopping detectors, respectively. In the above formula $b = B - \frac{C \cdot \Delta E}{D}$, B = 1.7943, $C = 4.2162 \cdot 10^{-2}\ \frac{\mu m}{MeV}$ and D denotes the thickness of the transmission detector in μm. The parameters B and C were adjusted to obtain identification parameter **p** practically energy independent. A typical identification spectrum obtained for $^{12}C+^{12}C$ system at beam energy of 344.5 MeV is presented in Fig. 1. Very good separation of the charge and mass of the ejectiles was obtained in the whole energy range covered by measurements.

The absolute values of cross section were evaluated from the measured counting rates, target thickness, solid angles of detecting system and integrated beam charge. The uncertainty in absolute normalization of the cross section was estimated to be 7% mainly due to the target thickness inaccuracy.

In the inclusive measurements the energy spectra of all stable ejectiles from ^4He up to ^{15}N were measured at laboratory angles covering the range from 4° to 11.5° in 0.5° steps and then to 36° in 1° steps. This range covers large part of the angular distributions. It follows from the identity of particles in the entrance channel that the cross section is symmetrical around 90° in centre of mass

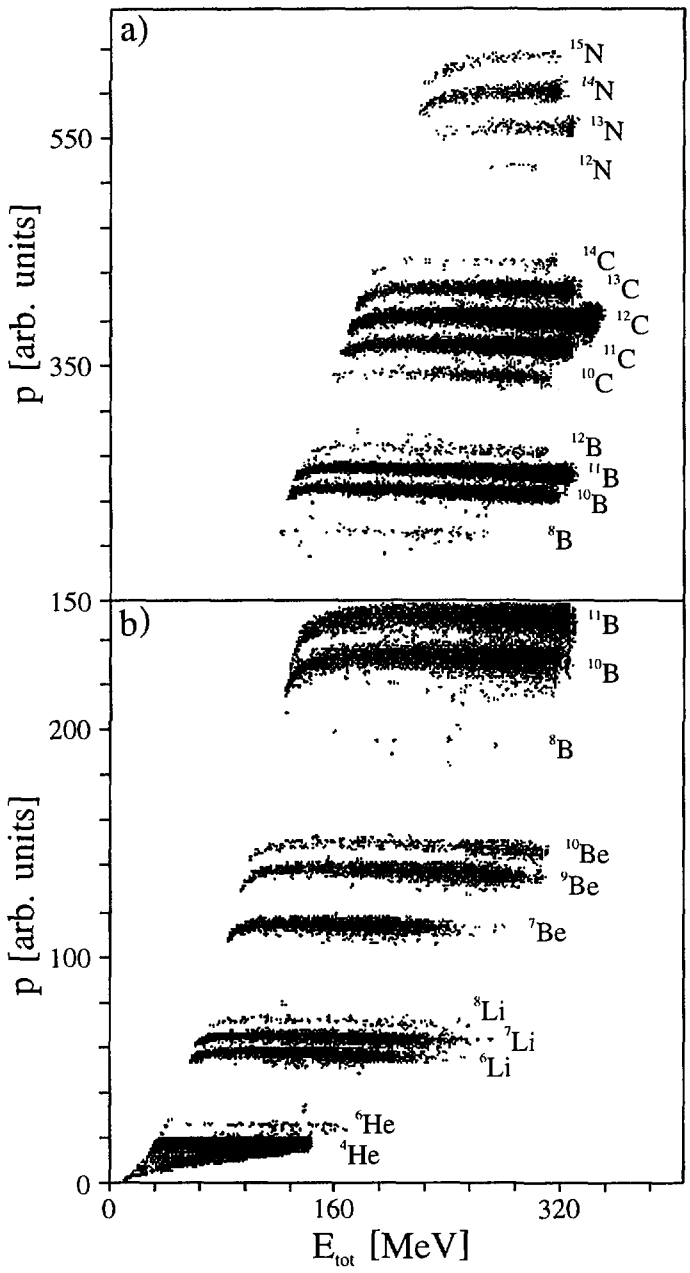

Fig. 1. An example of the identification spectrum for higher (a) and lower (b) mass ejectiles obtained for $^{12}C+^{12}C$ system at 344.5 MeV.

system (what corresponds to about 45° in laboratory system). Therefore the whole angular distribution may be obtained by measurements in laboratory angular range from 0° to about 45°.

The coincidences of various ejectiles were measured for angular configurations in a "close geometry" (+6°, –6°), (+6°, +11°) and in a "wide geometry" (+6°, –20°), (+6°, –30°). All telescopes were placed in the plane including the beam direction. The same sign of the angles refers to telescopes placed on the same side of the beam and different signs correspond to telescopes placed on the opposite side of the beam.

In the angular settings chosen for the coincidence measurements one of the telescopes was placed at small angle +6°. This telescope allows to detect the ejectiles produced in processes which are peaked at forward angles. Positions of the second detector cover the large part of the angular range. The coincidences observed in the "close geometry" will correspond mainly to the small relative energy of particles in coincidence, while the coincidences in the "wide geometry" correspond to larger relative energy of detected particles.

The high energy part of the spectra where peaks were observed was additionally measured using Big Karl spectrometer. This allowed better resolution of the discrete state transitions (with energy resolution of about 200 keV) and measurement at small angles down to 2°. The spectrometer was used also for the measurements of the Rutherford elastic scattering at small angles on ^{197}Au target in order to verify the absolute normalization of the cross section.

2.2. Results of inclusive measurements

Typical measured inclusive energy spectra are presented in Fig. 2 and 3. In Fig. 2 the energy spectra of ^{9}Be produced in the reaction ^{12}C(^{12}C, ^{9}Be) are shown for different laboratory angles. The energy spectra of different ejectiles ^{6}Li, ^{7}Be and ^{10}B produced at the same angle 5° (LAB) are presented in Fig. 3.

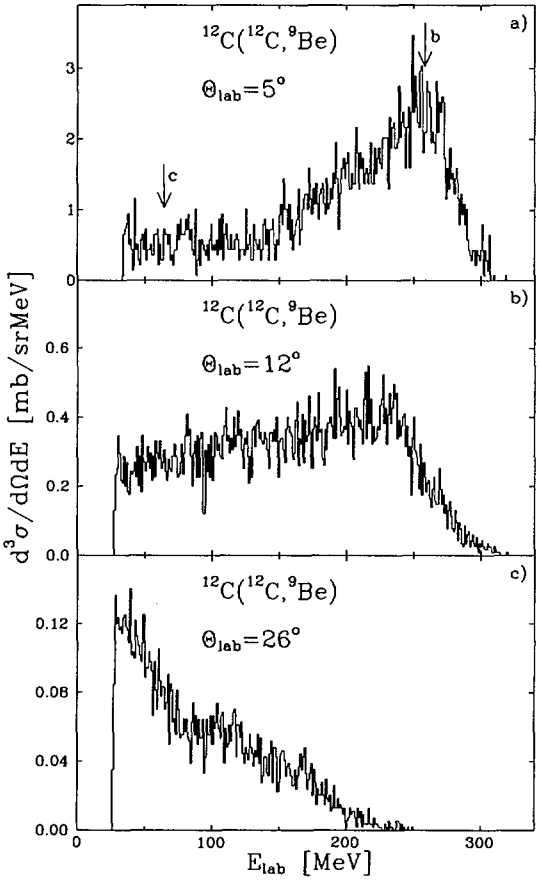

Fig. 2. Energy spectra of ^{9}Be measured for ^{12}C+^{12}C system at 344.5 MeV at various angles. Arrows labeled "b" and "c" indicate the ejectile energy corresponding to beam and centre of mass velocity, respectively.

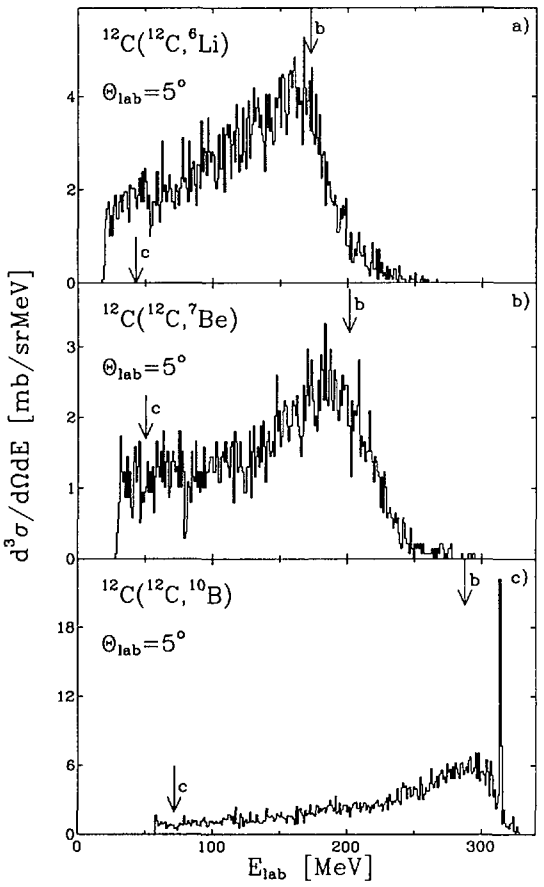

Fig. 3. Energy spectra of different ejectiles detected at 5° for $^{12}C+^{12}C$ system at 344.5 MeV. Arrows labeled "b" and "c" indicate the ejectile energy corresponding to beam and centre of mass velocity, respectively.

As may be seen from Fig. 2 and 3 the energy spectra at forward angles are dominated by the broad maximum located at energies close to those corresponding to the beam velocity marked with an arrow "b" in the figure. This maximum is asymmetric with a tail extending to small ejectile energies. At larger angles (see Fig. 2) this maximum practically disappears and spectra decrease strongly with the ejectile energy. At small energies where the contribution from the compound nucleus reaction may be expected (energies corresponding to the centre of mass velocity marked with an arrow "c" in Fig. 2 and 3) the observed cross section is small. The transitions to discrete states with definite excitation energies are also observed. As may be seen from Fig. 3 for outgoing ^{10}B few such transitions at small excitation energies are visible. They appear distinctly at small detection angles only. The strong excitation of single discrete states was seen in ^{13}N, ^{13}C, ^{12}C, ^{11}C, ^{11}B and ^{10}B spectra while week discrete states transitions appear in ^{10}C and ^{10}Be spectra. The observed discrete state transitions correspond to inelastic scattering and one and two nucleon transfer reactions.

The integrated cross sections obtained by summation of the experimental energy spectra over measured range of energy and angles are shown in Fig. 4 for all detected ejectiles. Peaks corresponding to the two body reactions were excluded from the integration. The integrated cross section for ^{4}He production exceeds by an order of magnitude the integrated cross section for all other

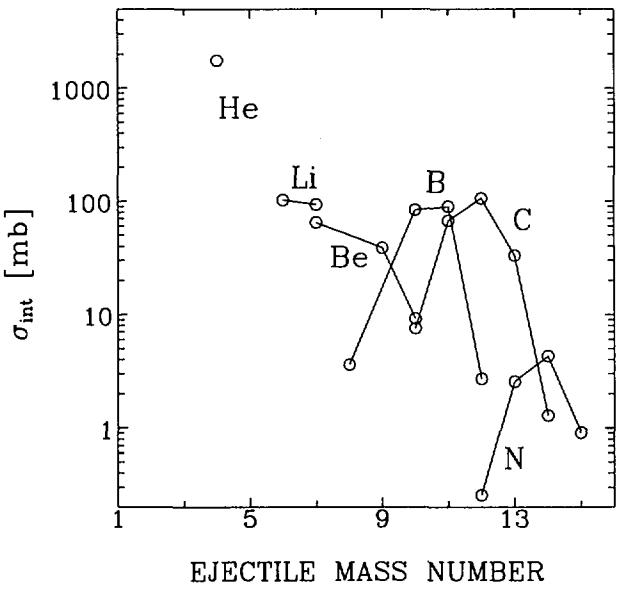

Fig. 4. Energy and angle integrated experimental cross section for all detected ejectiles as a function of atomic and mass numbers of the ejectile. Solid line connects different isotopes for separate elements. Peaks corresponding to the two body reactions were excluded from the integration.

ejectiles. For most ejectiles with mass smaller than the beam mass the integrated cross section is by factor of ca 100 larger than that for ejectiles with mass larger than beam mass. It suggests that the reaction mechanism leading to disintegration of the interacting nuclei dominates.

The examples of the observed angular distributions for the discrete state transitions and continuous part of the spectra are presented in Fig. 5. In Fig. 5a the angular distributions for the $^{12}C(^{12}C,^{10}B)^{14}N_{8.96}$ and $^{12}C(^{12}C,^{11}C)^{13}C_{3.85}$ reactions are shown, while in Fig. 5b the angular

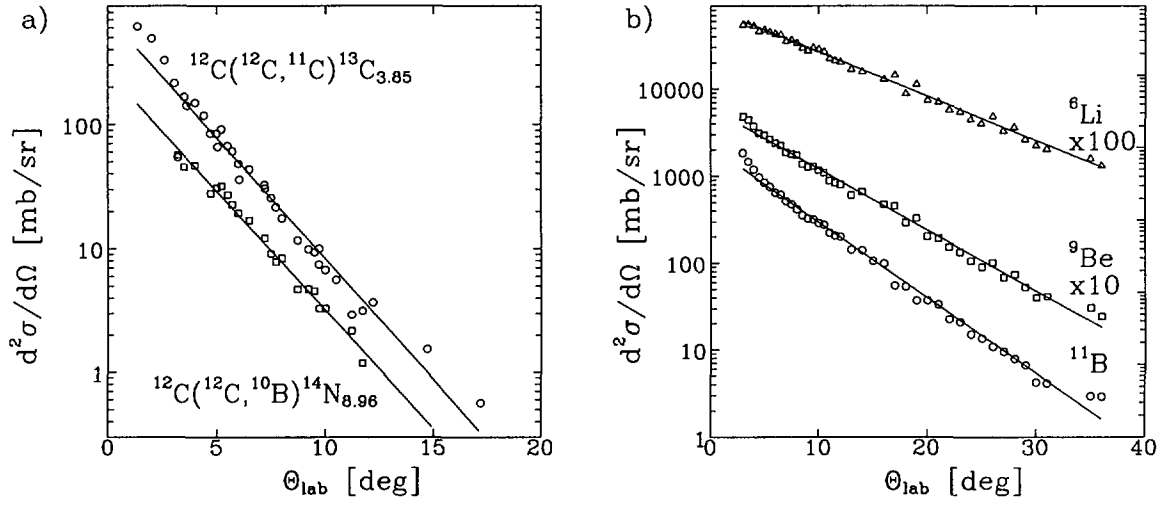

Fig. 5. Angular distributions obtained for $^{12}C+^{12}C$ system at 344.5 MeV. Left part (a) is for the angular distributions of $^{12}C(^{12}C,^{10}B)^{14}N_{8.96}$ (squares) and $^{12}C(^{12}C,^{11}C)^{13}C_{3.85}$ (circles) reactions. Right part (b) is for energy integrated continuous spectra of outgoing ^{11}B (circles), ^{9}Be (squares) and ^{6}Li (triangles). Exponential functions plotted were fitted separately for each angular distribution using least square method.

distributions of energy integrated (over measured energy range) continuous part of experimental spectra of outgoing ^{6}Li, ^{9}Be and ^{11}B are presented. The common feature for these distributions is their exponential dependence on the ejectile laboratory angle. The exponential function obtained with the least square method for each angular distribution is also plotted to show this dependence of experimental points.

2.3. Results of coincidence measurements

The typical coincidence patterns are shown in Fig. 6, 7 and 8 as the two dimensional plot of the intensity in function of the coincident fragments energy for a given angular configuration. The coincidence spectra presented in Fig. 6 and 7 are for "close geometry" i.e. angle settings (+6°, –6°) and coincidences of α–^{10}B and α–^{6}Li, respectively, that in Fig. 8 are for "wide geometry" angular setting (+6°, –30°) for coincidences of α–^{6}Li. The kinematical curve calculated from energy and momentum conservation for the corresponding three body reaction ^{12}C(^{12}C,α^{10}B)^{10}B for α–^{10}B and ^{12}C(^{12}C,α^{6}Li)^{14}N for α–^{6}Li coincidences was also plotted. This curve defines the limits for the kinetic energy of particles in coincidence. The events situated on the kinematical curve correspond to the three body reaction with all particles in the ground state, events lying inside the region enclosed by this curve may be accounted to the excitation of ejectiles or to more than three body reaction. Events outside this region correspond to random coincidences only.

As it is seen from Fig. 6, 7 and 8 three qualitatively different coincidence patterns are observed. In Fig. 6 the majority of the coincidence events are concentrated close to the kinematical curve calculated for the ^{12}C(^{12}C,α^{10}B)^{10}B three–body reaction with all final state particles in the ground states. Beyond the vicinity of kinematical curve some events are observed for ejectile energies

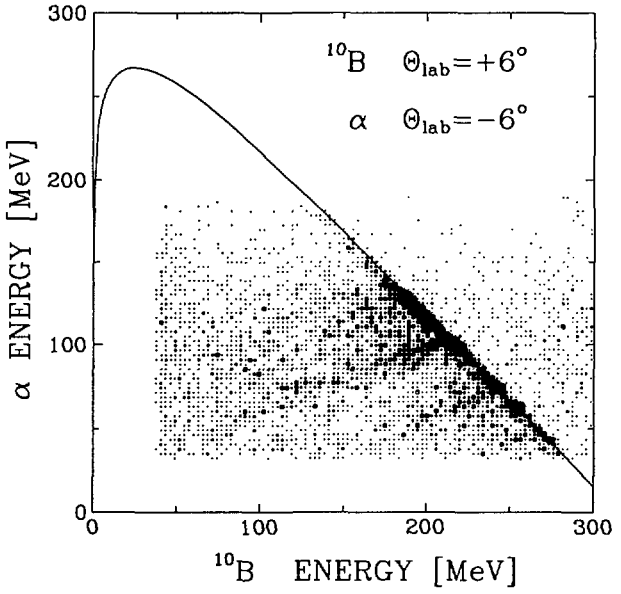

Fig. 6. Two-dimensional spectrum for α–^{10}B coincidences for angular configuration (+6°,–6°) for ^{12}C+^{12}C system at 344.5 MeV. The density of the points corresponds to the magnitude of the cross section and varies logarithmically. Solid curve represents the ejectiles energies that correspond to a three body reaction with all final state particles in their ground states (kinematical curve).

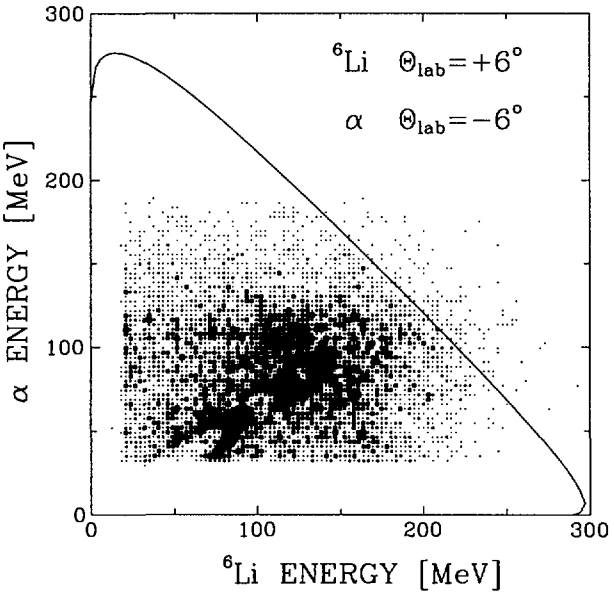

Fig. 7. Similar as in Fig. 6 but for α–^{6}Li coincidences for angular configuration (+6°,–6°).

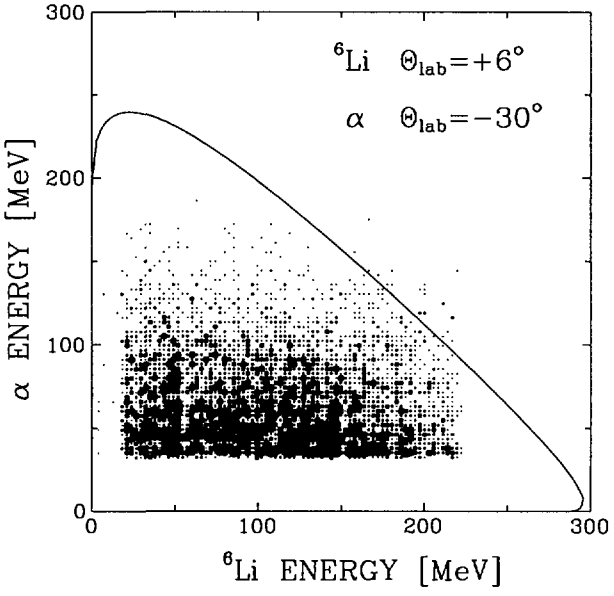

Fig. 8. Similar as in Fig. 6 but for α–^{6}Li coincidences for angular configuration (+6°,–30°).

smaller then those for kinematical curve. Such type of coincidence pattern is dominating for α+^{9}Be and α+^{10}B coincidences in "close geometry". Second type of observed coincidence pattern is presented in Fig. 7. It is characterized by majority of coincidence events with ejectile energies much smaller than those corresponding to the kinematical curve. These coincidence events are, however, not distributed randomly but they are correlated to some curves. Similar behavior of the coincidence cross section is observed also for α–^{7}Be, α–^{7}Li, α–^{6}Li and α–α coincidences in "close geometry". The third type of coincidence patterns appears for "wide geometry" coincidences. As may be seen for a typical example in Fig. 8 the coincidence events for "wide geometry" are concentrated at small energies of both detected ejectiles and do not group close to the kinematical curves as for "close

geometry" measurements. For the "wide geometry" measurements the coincidence patterns for all α–heavier ejectile coincidences are very similar.

2.4. Reactions with identical particles in the entrance channel

Before proceeding with the analysis of reaction processes, the advantages of the reactions with identical particles in the entrance channel will be discussed. For identical projectile and target nuclei the processes with excitation of projectile or target like nuclei are undistinguishable. In such case it is not necessary to detect very low energy particles (target like nuclei) or to do measurements in inverse kinematic. In order to obtain the information about all occurring processes it is sufficient to measure in the forward hemisphere and detect particles with large energies originating from the projectile like nuclei only. It is illustrated in Fig. 9 for one nucleon transfer reaction followed by particle decay. This process is shown schematically in the centre of mass system. As it follows from Fig. 9 the entrance channel particles identity allows observation of excitation of unbound states (process a) and the decay products of these states after the particles emission (process b) by detection of ^{11}B and ^{12}C ejectiles in the forward hemisphere. The entrance channel particles identity results in the fore–aft symmetry of the cross section in the center of mass system. Thus in example shown in Fig. 9 the cross section for production of ^{11}B and $^{13}N^*$ ejectiles are equal for given c.m. angle

$$\frac{d^2\sigma\,^{11}B(\theta_{cm})}{d\Omega} = \frac{d^2\sigma\,^{11}B(\pi-\theta_{cm})}{d\Omega} = \frac{d^2\sigma\,^{13}N^*(\theta_{cm})}{d\Omega}$$

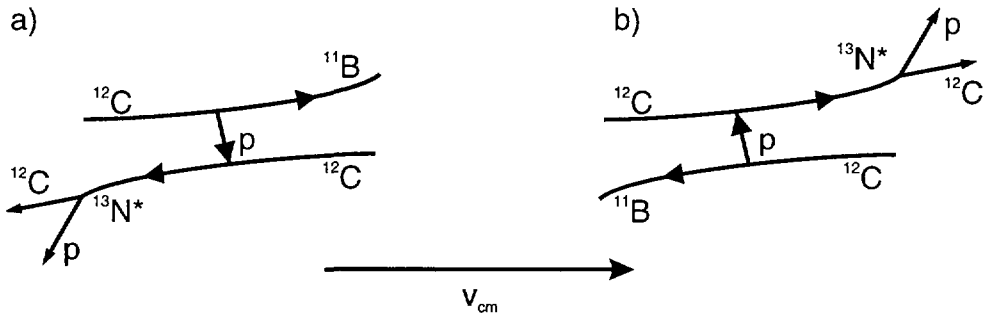

Fig. 9. Schematic representation of one nucleon transfer process. On the left plot the ^{11}B nucleus is detected in the forward direction, while on the right one the decay product ^{12}C nucleus is detected in the forward cone.

Therefore measured one nucleon transfer cross section (by detection of ^{11}B in forward hemisphere – process a) is exactly equal to the production cross section for unbound $^{13}N^*$ nuclei. In this way we determine the first step of the sequential process consisting of transfer reaction with subsequent decay of the one product (process b). Using the measured cross section for ^{11}B ejectiles the production of ^{12}C nuclei in the entire reaction may be obtained. The above arguments are valid only if in the first stage of reaction one of both product nuclei is emitted in a bound state.

3. Analysis of compound nucleus, inelastic excitation and transfer reactions

At small incident energies the reactions in the system of light heavy ions (e.g. $^{12}C+^{12}C$ system) are dominated by compound nucleus and direct processes (i.e. inelastic scattering and transfer reactions)[79,80,81,82]. Prior to consideration of other more complicated reaction mechanism that may appear at intermediate incident energy, the contributions of these known mechanisms have to be regarded, so more that direct reactions are expected to be initial step for some sequential processes.

3.1. Compound nucleus reactions

To evaluate the contribution of the compound nucleus reaction to the spectra of various ejectiles the calculations of the evaporation from compound nucleus were performed using the PACE code[83]. The resulting cross section depends on the parameters in level density formula and on the maximum angular momentum l_f for fusion.

For the calculations of level density the Gilbert–Cameron parameterization[84] was used. It contains two basic parameters: level density parameter **a** and pairing energy. The common parameterization of level density parameter $\mathbf{a} = A/5$ (A is nucleus mass number) and the pairing energy parameterization proposed in ref. 85 were used. The same parameters were successfully used in an extended analysis of $^{9}Be+^{12}C$ fusion at E_{cm}=11.4 MeV[86] and $^{11}B+^{12}C$ at E_{cm} = 36.5 and 41.7 MeV[87,88] where the same nuclei as in the present analysis appear in the compound nucleus decay.

In order to estimate the maximum angular momentum for fusion the potential model was used[89,90]. According to this model the maximum angular momentum l_f for fusion corresponds to the angular momentum l_{crit} for which the "pocket" in the total potential (coulomb, nuclear and centrifugal) disappears at sufficiently high beam energy (a few tens of MeV) . Using the optical model potential determined for $^{12}C+^{12}C$ system[74] the value of $l_f=l_{crit}=17$ was obtained. This value leads to fusion cross section of 200 mb what is in a good agreement with the predictions of the Porto-Sambataro phenomenological model[91] resulting in fusion cross section value equal 180 mb. The obtained value of fusion angular momentum is below value at which the fission barrier vanishes[92].

As an example the results of these calculations for ^{10}B and α particles ejectiles are compared with experimental energy spectra in Fig. 10 and 11 for some angles. The obtained cross section for outgoing ^{10}B produced as the evaporation residuum accounts for a large portion of the experimental cross section at small ejectile energies and small angles only. The contribution of the evaporation residuum cross section decreases with increasing angle and becomes very small in relation to the experimental cross section at laboratory angles larger than 30°. Similar behavior is observed for all other evaporation residua. As shown in Fig. 11 the cross section for α particles evaporated in the decay of compound nucleus is small in relation to the experimental data at small angles, while accounts for about 20% of the experimental cross section at larger angles.

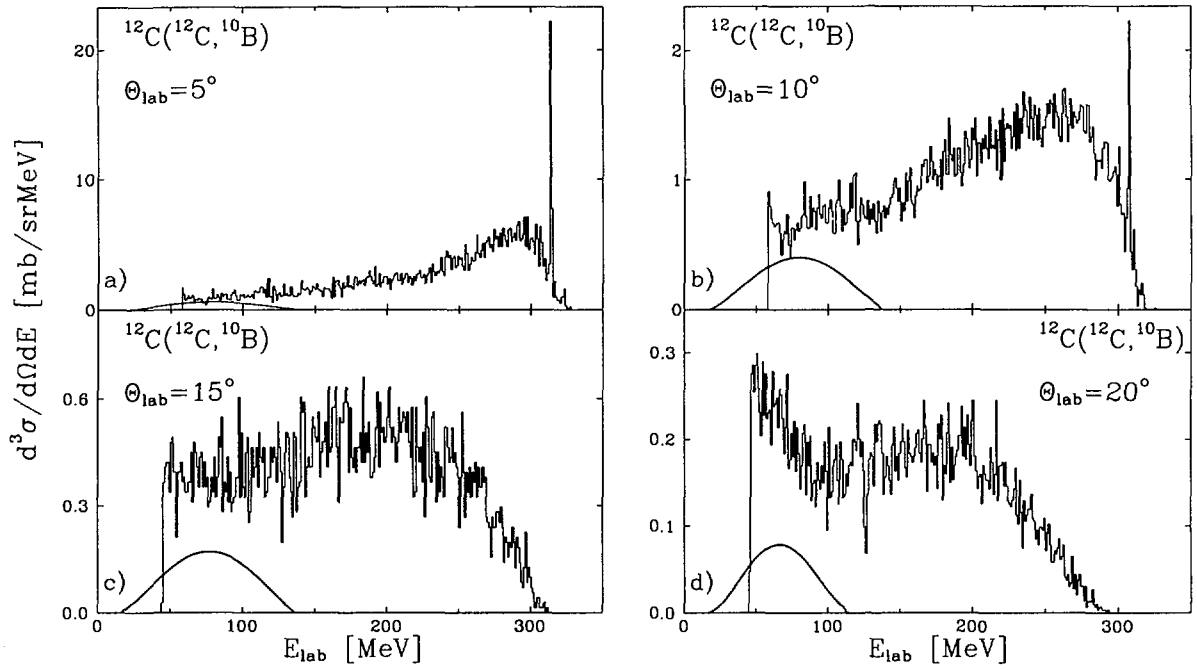

Fig. 10. Energy distributions (histograms) of outgoing ^{10}B nuclei for selected angles compared with statistical model calculations (solid line).

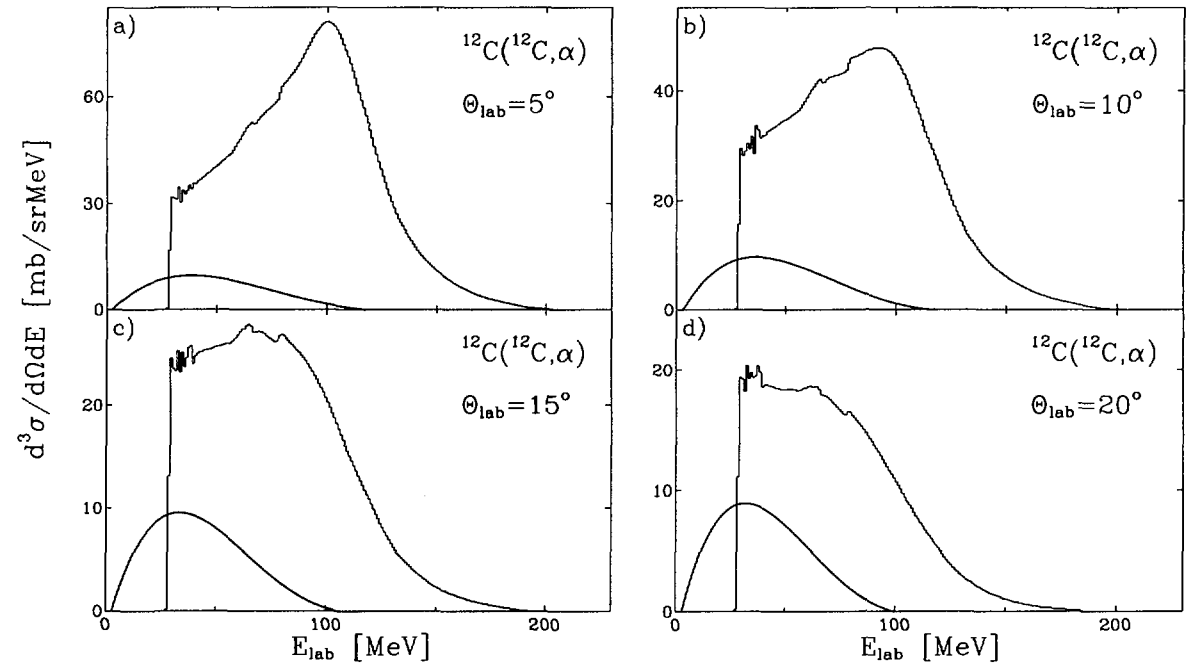

Fig. 11. Energy distributions (histograms) of outgoing α particles for selected angles compared with statistical model calculations (solid line).

3.2. Analysis of discrete states transitions

For the investigated $^{12}C+^{12}C$ incident channel the reactions with one and two nucleon transfer and inelastic excitation leading to discrete states were observed. A few excited states with an excitation energy up to 10 MeV were identified, some of them being unbound states. Mutual excitations of projectile like and target like nuclei were also seen. From the experimental cross section it follows that the transfer probability decrease with the increasing number of transferred nucleons. Indeed the deuteron transfer to only one state is observed with considerable strength, and its probability is smaller than for one nucleon transitions. Other two nucleon (two neutron and two proton) transfers appear with negligibly small strength. The three nucleon transfer and α particle transfer were not observed. This agrees with the semi-classical considerations based on Brink model[93,94], which suggests that kinematic matching conditions are not fulfilled for α particle transfer at beam energy of the present experiment[95].

The detailed analysis of the elastic scattering (with optical model) and inelastic one to the first ^{12}C excited state as well as one nucleon transfer reactions leading to discrete bound and unbound states of final nuclei (using DWBA) was performed. The results of the analysis were presented in ref. 74,75,95. Very good reproduction of the experimental angular distributions for these reactions was obtained as may be seen in Fig. 12 for exemplary angular distribution. The values of potential deformation length deduced from the analysis of inelastic scattering as well as one nucleon spectroscopic factors for states excited in one nucleon transfer agree very well with those from the other studies at low incident energies. Similar analysis of two nucleon transfer[95] indicates that it proceeds as a correlated transfer.

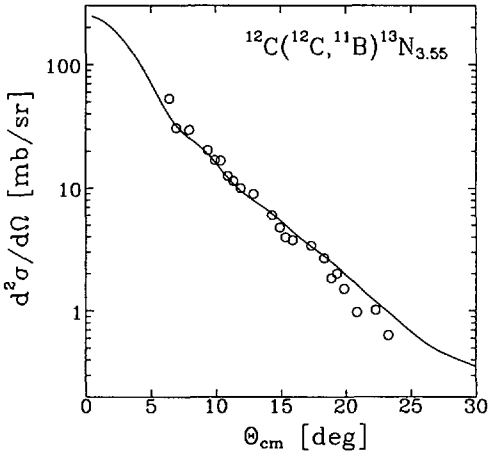

Fig. 12. Angular distribution for $^{12}C(^{12}C,^{11}B)^{13}N_{3.55}$ reaction compared with DWBA calculations.

The analysis of transitions to the discrete states shows that direct processes (inelastic excitation and transfer) are still very important at intermediate energies. It may be expected that these reactions may also lead with large probability to region of high excitation energies where large density of states appears. The accurate analysis of the direct processes leading to high excited states is of special interest, since they are unbound and subsequently decay through the particle emission contributing to many particles exit channels, corresponding to sequential fragmentation processes.

3.3. Simple example of sequential process

A good example of the sequential process is the decay process initiated by transfer reaction. The excitation of 8.96 MeV ^{14}N state in deuteron transfer reaction and its subsequent proton decay will be regarded. Schematically this process is presented in Fig. 13. The deuteron transfer to 8.96 MeV ^{14}N state leads to a strong peak in ^{10}B spectrum presented in Fig. 3c, 10a and 10b. The experimental angular distribution obtained for this transition (shown in Fig. 5a) was well reproduced by DWBA calculations[95]. The 8.96 MeV ^{14}N state is unbound and decays by the proton emission with 100% probability since other decay channels are closed due to their energy thresholds larger than 9 MeV. Due to the symmetry with identical particles in the entrance channel it is possible to obtain directly the cross section for both (^{10}B and ^{14}N*) outgoing particles by detecting ^{10}B ejectiles only. Therefore the angular distribution measured for ^{10}B (Fig. 5a) could be used to obtain formation probability of ^{14}N* nucleus in the forward hemisphere in the first stage of reaction. Assuming that decay is isotropic in the rest frame of decaying ^{14}N* nucleus the $\frac{d^3\sigma}{d\Omega dE}(E, \theta)$ cross section for outgoing ^{13}C nuclei produced in sequential decay process may be calculated without free parameters. The results of these calculations are presented in Fig. 14. In the kinematically allowed region the contribution of the sequential process, described above, to the continuous part of ^{13}C spectra is significant. That confirms the importance of the sequential processes initiated by transfer reactions. At larger angles the calculated cross section accounts only for part of the experimental cross section for ^{13}C nucleus. This suggests that transitions to higher excited states of ^{14}N nucleus have to be taken into consideration. Higher excited levels have in laboratory system larger decay cone and therefore they contribute significantly at larger emission angles, and their decay lead to broader laboratory energy distributions of ejectiles.

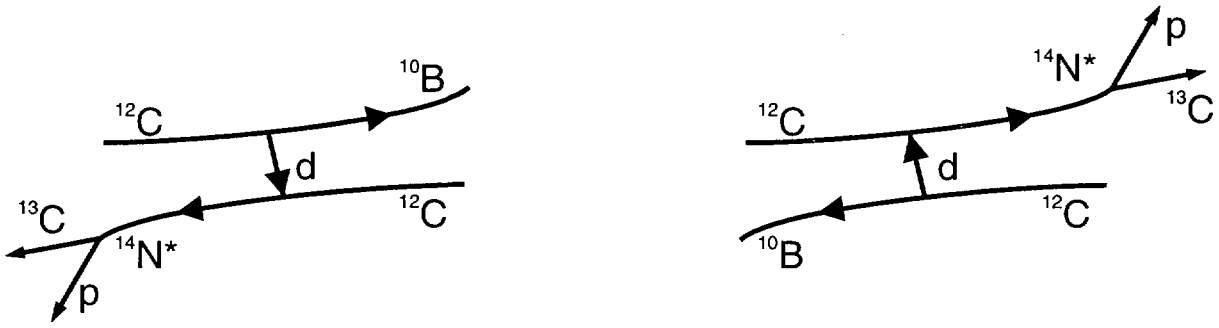

Fig. 13. Schematic representation of deuteron transfer reaction $^{12}C+^{12}C \rightarrow {}^{10}B+{}^{14}N^*$ and a subsequent proton decay of excited state $^{14}N^* \rightarrow p+{}^{13}C$.

3.4. Inelastic scattering and one nucleon transfer leading to high excited states

The direct processes leading to high excitation energies are in part responsible for the observed continuum energy distribution. As discussed above they initiate sequential decay process in which various ejectiles may be produced. Therefore the analysis of direct processes leading to the continuum of states is required.

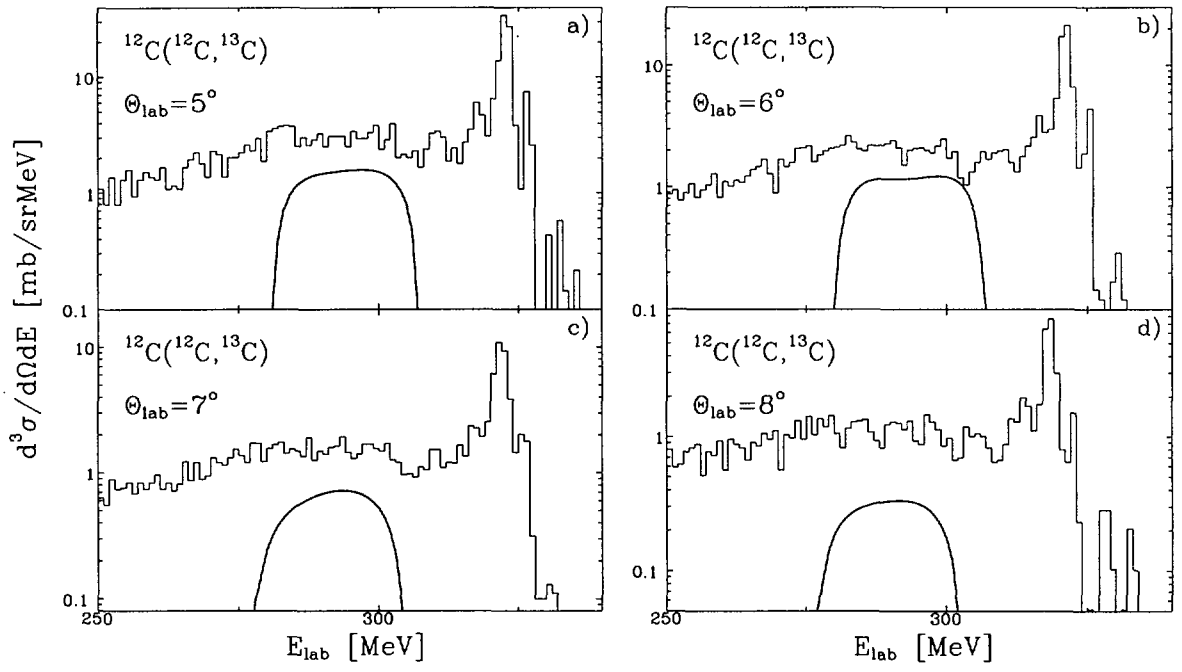

Fig. 14. The experimental energy spectra for outgoing ^{13}C compared with sequential process calculations (solid line) as described in the text.

Detailed microscopic calculations of inelastic excitation and one nucleon transfer reactions leading to high excitation energies were performed[76,77]. The analysis of the inelastic scattering process was done basing on the Multistep Direct Reaction (MSDR) theory[96]. The MSDR theory is an extension of DWBA model to the excitation energy range where many various states are excited and statistical features dominate. The main feature of the MSDR approach is the expansion of real nuclear states into classes of model states of increasing complexity. Expansion coefficients are treated stochastically and thus the transitions proceed as incoherent multistep process. Density expansion method QRPA (Quasiparticle Random Phase Approximation) is used for the calculation of nuclear structure. The evaluation of transition matrices is done in frame of DWBA i.e. the first or higher order perturbation theory. Though MSDR theory allows the calculations of high order transitions, already the calculation of the third order processes becomes cumbersome. For details about MSDR theory and the inelastic scattering calculations in the frame of MSDR theory see ref. 76 and 77 where the calculations up to second order are presented for $^{12}C+^{12}C$ system. The results of the MSDR calculations are shown in Fig. 15 together with the experimental data. As may be seen from Fig. 15 only the high energy part of the ^{12}C spectra corresponding to not very high excitation energy (up to a few MeV excitation energy) is well described by the MSDR calculations. In this region some peaks are visible, which correspond to the projectile or target excitation, or to the mutual projectile and target excitations. The observed excitations have to be attributed mainly to the target excitations. Projectile have only one bound excited state (4.44 MeV), and excited to the energy larger

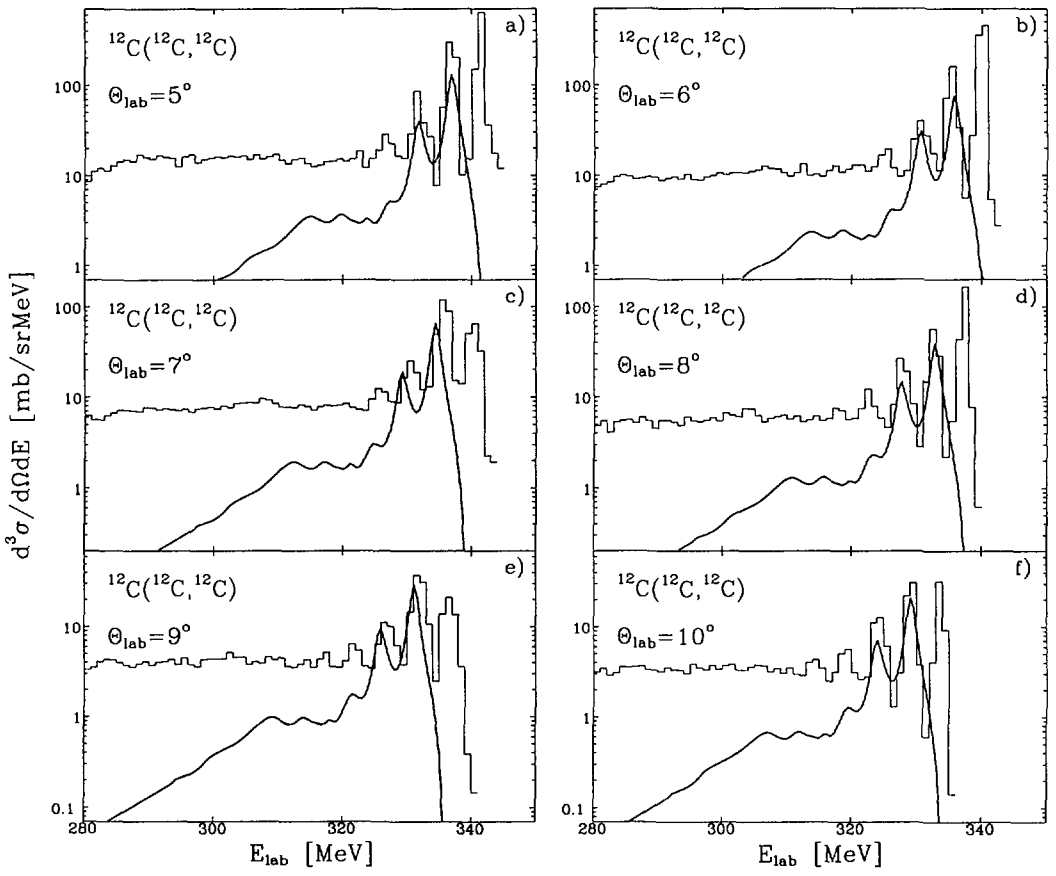

Fig. 15. Energy distributions of outgoing ^{12}C at various angles. Thick solid lines correspond to MSDR calculations of inelastic processes as described in the text. The peaks at largest energy correspond to the elastic scattering.

than 7.4 MeV decays and cannot be detected as ^{12}C nucleus. The inelastic excitations proceed via one or two step processes whose contributions at excitation energies above 10 MeV are of almost the same magnitude. At higher excitation energies (smaller ^{12}C ejectile energies) the calculations underestimate the experimental cross section. More likely the missing cross section is related to the three or more step inelastic process. It may be attributed also to transfer processes followed by the decay, what will be discussed in the next section.

The one nucleon transfer reactions leading to continuum spectrum of unbound states were also analysed[77]. The analysis was performed in framework of one step DWBA with form factors calculated for the continuum single particle states[97]. The transfer strength functions, for one nucleon configurations in ^{13}N and ^{13}C nuclei, were calculated microscopically in the quasiparticle core coupling model (QPC)[98,99]. The results of the calculations taken from ref. 77 are compared with the experimental data in Fig. 16. The calculated cross section may account for the experimental one only in rather small part of the spectra at large ejectile energies. The peaks visible in the spectra correspond to excitation of ^{13}C or ^{13}N states and were analysed separately[75]. At lower outgoing energies the calculated cross section underestimates data by a large factor.

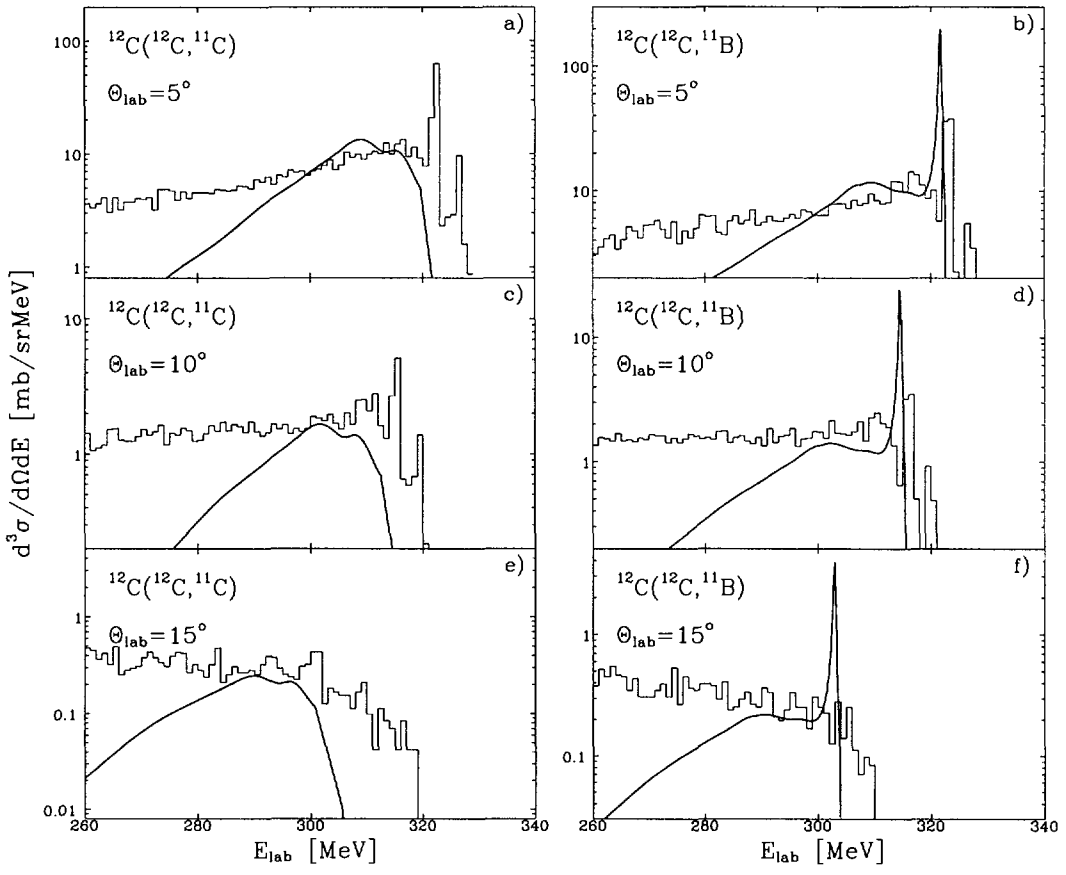

Fig. 16. Energy distributions of outgoing ^{11}C and ^{11}B for various angles. Thick solid lines correspond to DWBA calculations of one nucleon transfer processes as described in the text.

3.5. Sequential one nucleon decay of ^{13}N and ^{13}C excited in one nucleon transfer reactions

A large part of ^{12}C spectra cannot be described by second order inelastic scattering calculations. The one nucleon transfer to unbound states (discussed above) followed by nucleon decay may be responsible for part of this missing cross section. In the nucleon transfer reactions the states with large one nucleon spectroscopic factor are preferentially excited and therefore have predominantly structure with ^{12}C core. Such unbound states decay with large probability by nucleon emission. Therefore it may be assumed that decay probability of these states by nucleon emission is equal to one. Additionally it is assumed that decay is isotropic in the rest frame of decaying nucleus. At excitation energies of a few MeV many different states with various spin and therefore various alignment are excited. It may be expected that for such states alignment averaged over excitation energy is equal zero, what leads to the isotropy of their decay. Under these assumptions and using calculated one nucleon DWBA transfer cross section for the first stage of the reaction, the distributions of ^{12}C ejectiles produced in sequential process may be calculated without free parameters. The results of this analysis are presented in Fig. 17 (dashed line) together with experimental data. It is seen that sequential process started by one nucleon transfer reaction and inelastic scattering (solid line in Fig. 17) may describe high energy part of experimental ^{12}C spectra.

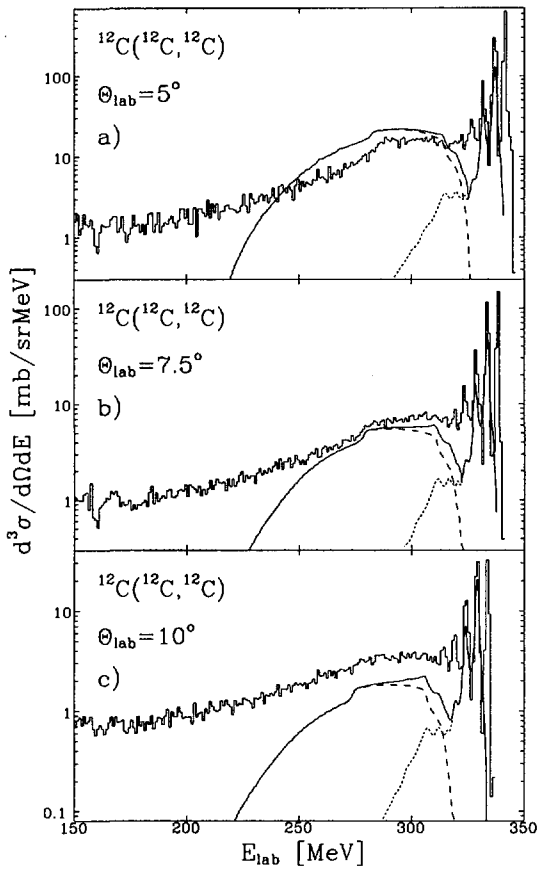

Fig. 17. Energy distributions of outgoing ^{12}C at various angles. Dashed lines correspond to the calculations of the sequential process initiated by nucleon transfer. Solid lines correspond to the sum of sequential process calculations and MSDR calculations of inelastic processes (dotted lines).

However, there remains still some part of cross section at low ^{12}C ejectile energy that cannot be explained by such processes. It corresponds partly to the ^{12}C nuclei produced as the evaporation residua of the compound nucleus. Some part of this missing cross section could be also attributed to the inelastic scattering process of higher orders than those taken into account in the calculations.

3.6. Summary of results of compound nucleus and direct reactions analysis

Various ejectile spectra were analysed by means of compound nucleus and direct reaction models. It was shown that ejectiles produced in compound nucleus decay have distributions concentrated at small energies, close to the energy corresponding to the centre of mass velocity. The calculated cross section for ejectiles produced as the evaporation residua of compound nucleus may account for some part of the experimental cross section only. Similar observation holds for calculated α particles distributions which are evaporated from compound nucleus.

The excitation of discrete states in inelastic scattering (^{12}C spectra) and one nucleon transfer reactions (^{11}C and ^{11}B spectra) was analysed using DWBA. Very good reproduction of the experimental data was obtained with parameters consistent with analysis at low incident energies. The transitions to higher excited states in inelastic process were analysed with second order MSDR

theory and QRPA method for nuclear structure calculations. One nucleon transfer leading to continuum unbound states of ^{13}N and ^{13}C nuclei was analysed using first order DWBA and QPC model for strength function calculations. It was shown that these microscopic calculations may account for part of the experimental cross section for ^{12}C nuclei (inelastic process) and ^{11}B and ^{11}C ejectiles (transfer reactions) at large outgoing energies.

The analysis of the deuteron transfer to unbound ^{14}N 8.96 MeV state followed by proton decay was performed without free parameters. It was shown that such process contributes significantly to ^{13}C ejectile spectra. The ^{12}C ejectile production in sequential process was analysed. Using calculated excitation probabilities of unbound ^{13}N and ^{13}C states and regarding their nucleon decay the ^{12}C distributions were calculated without free parameters. These sequential processes may account for the appreciable part of ^{12}C ejectile experimental cross section at large outgoing energies.

A large portion of experimental energy spectra for other ejectiles (α particles, ^{6}Li, ^{7}Li, ^{7}Be, ^{9}Be, ^{10}B, ^{11}B and ^{11}C) can be described neither by inelastic excitation nor by transfer processes and compound nucleus reactions. Performed analysis suggests that direct processes leading to unbound states followed by the decay with emission of various particles may be responsible for missing cross section for these ejectiles.

4. Kinematical signatures of the sequential fragmentation reactions

As shown in the previous section various processes (compound nucleus, direct and sequential reactions) lead to continuum distribution in the inclusive spectra. Therefore they cannot be distinguished without comparison of the inclusive data with some model calculations. Since the coincidence data contain more information than the inclusive ones it may be expected that model independent conclusions about reaction mechanism may be drawn from their analysis. Therefore the characteristic features of measured coincidence patterns will be discussed basing only on kinematical considerations in order to obtain model independent information about the reaction mechanism.

The coincidence cross section $\frac{d^6\sigma}{dT_1 d\Omega_1 dT_2 d\Omega_2}$ as a function of laboratory kinetic energies T_1 and T_2 and laboratory angles Ω_1 and Ω_2 of particles 1 and 2 detected in coincidence was measured. As it is seen from Fig. 6 and 7 the coincidence events are not distributed homogeneously but are grouped for specific values of T_1 and T_2 energies. Observed correlation may be caused by formation of intermediate excited states or by energy sharing between ejectiles. In order to analyse these properties it is convenient to introduce some variables for representation of coincidence cross section. For the reaction

$$a + b \rightarrow 1 + 2 + \ldots + n \qquad n = 3, 4, \ldots$$

with known masses m_i and four momenta p_i of beam – a, target – b nuclei and two detected in coincidence ejectiles – 1 and 2 the following variables were defined:

1. Excitation energy E^*_{12} of the system composed of ejectiles 1 and 2 is defined by

$$E^*_{12} = \sqrt{(p_1 + p_2)^2} - m_{12}$$

where m_{12} is mass of nucleus composed of nucleons of particle 1 and 2 (e.g. for α–^{9}Be coincidences m_{12} is the mass of ^{13}C nucleus). When in the reaction particles 1 and 2 form the composed system in the resonant state, peaks corresponding to the excitation energy of this state should be visible in the coincidence cross section represented as a function of E^*_{12}.

2. Missing energy Q_3 (energy not observed when detecting only particles 1 and 2) is defined by

$$Q_3 = \sqrt{p_x^2} - m_x = \sqrt{(p_a + p_b - p_1 - p_2)^2} - m_x$$

where p_x is four momentum of all unobserved particles ($p_x = p_3 + \ldots + p_n$) and m_x is the unobserved mass. Mass m_x correspond to mass of nucleus with number of neutrons N and protons Z calculated from the conditions $N=N_a+N_b-N_1-N_2$ and $Z=Z_a+Z_b-Z_1-Z_2$ (e.g. for ^{12}C(^{12}C,α^6Li) reaction N=7 and Z=7 and therefore m_x is ^{14}N nucleus mass). The missing energy in case of three body reactions may

be converted into excitation energy of outgoing particles, or in case of more than three body process into a kinetic energy and excitation energy of unobserved ejectiles.

For the analysis of coincidence data the detector system efficiency have to be known. The efficiency depends on angular configuration of detectors, relative velocity and the sum of velocities of particles in coincidence (hence depends on E^*_{12} and Q_3). For each analysed angular configuration efficiency was calculated using Monte Carlo method, taking into account solid angles of the detectors used in the measurements. An example of the calculated efficiency is shown in Fig. 18a for α–^{6}Li coincidences for (+6°, +11°) angular configuration. Its dependence on excitation energy E^*_{12} and missing energy Q_3 is shown in Fig. 18b and 18c for investigated angular configurations. It is seen that the efficiency strongly decrease with increasing E^*_{12} value and that for various angular configurations the different E^*_{12} regions are observed with large efficiency. The efficiency does not depend strongly on the missing energy Q_3 value and is practically constant in the whole available Q_3 range.

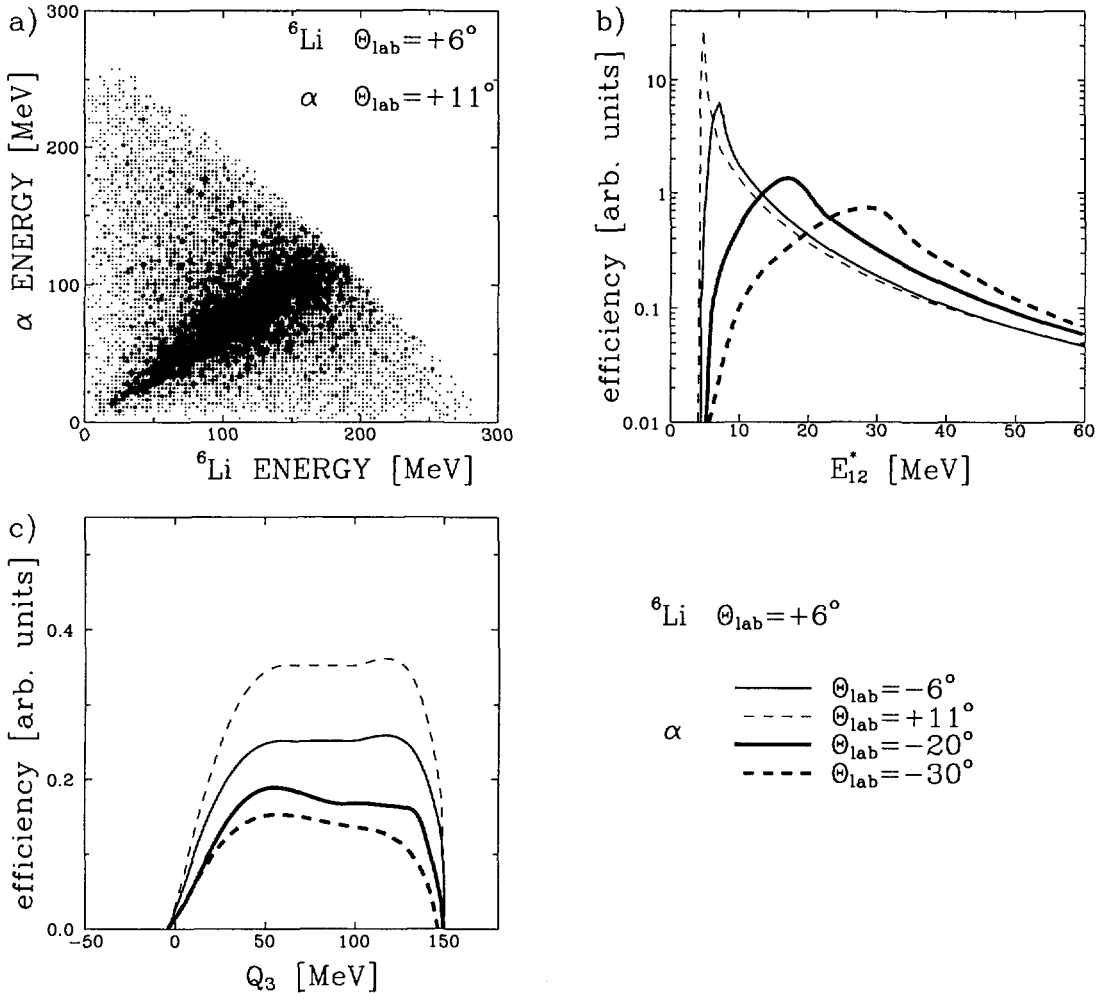

Fig. 18. Two-dimensional plot of the calculated efficiency for α–^{6}Li coincidences for (+6°,+11°) angular configuration (a). The efficiency as the function of excitation energy E^*_{12} (b) and missing energy Q_3 (c).

4.1. Model independent analysis of coincidence spectra

The analysis of the coincidence data based only on the kinematical considerations was performed. Such analysis offers the possibility to deliver model independent information about the reaction mechanism.

As examples the α–^{9}Be and α–^{10}B coincidences may be regarded. The experimental α–^{9}Be coincidence spectra for (+6°, +11°) angular configuration are presented in Fig. 19a. It is seen that most of the coincidence events are concentrated on the kinematical curve corresponding to α+^{9}Be+^{11}C final state with all outgoing particles in ground states. Such coincidences corresponding to three body reaction may originate in the processes schematically represented in the centre of mass system by diagram in Fig. 20.

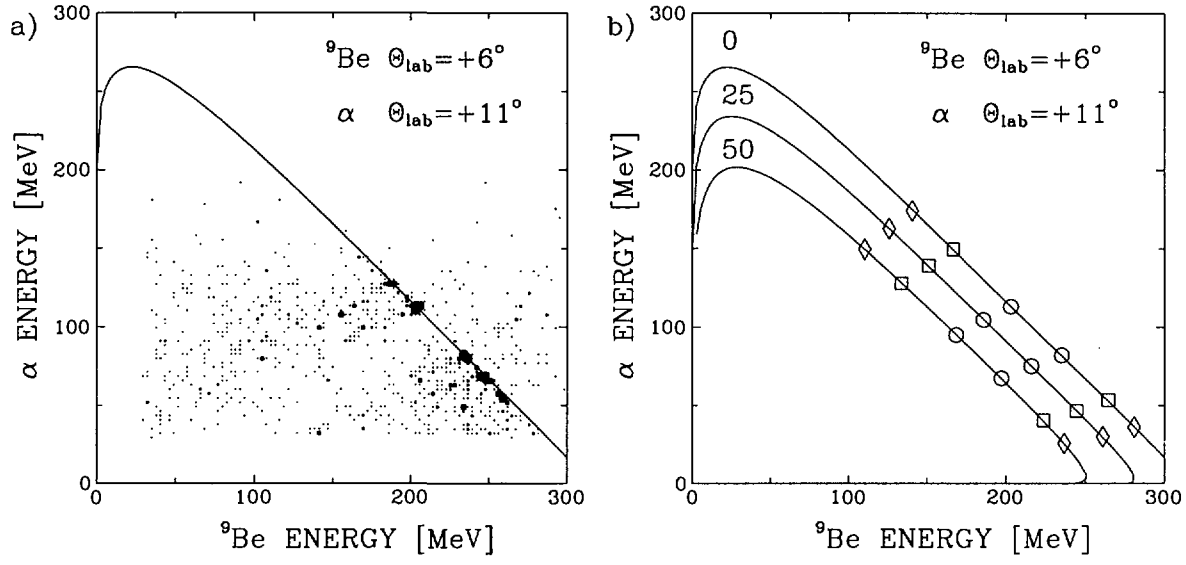

Fig. 19. Two-dimensional spectrum for α–^{9}Be coincidences for angular configuration (+6°,+11°) (a). Solid curve represents the ejectiles energies that correspond to a three body reaction with all final state particles in their ground states (kinematical curve). In part (b) the kinematical curves for various values of missing energy Q_3 (solid lines with labels corresponding to Q_3 values in MeV) and some selected values of excitation energy E^{*}_{12} (circles for 12 MeV, squares for 20 MeV and diamonds for 30 MeV) for three body reaction ^{12}C(^{12}C,α^{9}Be)^{11}C.

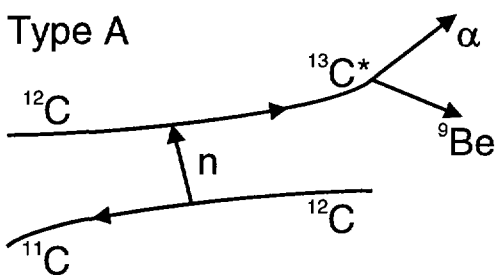

Fig. 20. Schematic representation of neutron transfer reaction ^{12}C+^{12}C → ^{11}C+^{13}C* and a subsequent α particle decay of excited state ^{13}C* → α+^{9}Be.

In the neutron transfer reaction the ^{13}C and ^{11}C nuclei are produced. The ^{13}C nucleus may be excited to the energy larger than the threshold energy for α particle emission. Therefore this nucleus decays subsequently into α particle and ^{9}Be nucleus. In case of such three body $^{12}C(^{12}C,\alpha^{9}Be)^{11}C$ reaction the α–^{9}Be coincidence events will be distributed along the kinematical curve for appropriate Q_3 value corresponding to excitation of final particles. The ^{9}Be nuclei in excited states cannot be detected since ^{9}Be does not have bound excited states. Therefore in the case of three body reaction various Q_3 values should be attributed to excitation of ^{11}C nucleus. As examples the curves corresponding to the various Q_3 values for α–^{9}Be coincidences for (+6°, +11°) angular configuration are shown in Fig. 19b as the solid lines. The relative importance of the three body reactions is well visible in Fig. 21 where the coincidence cross section is shown as function of missing energy Q_3. The peak at Q_3=0 correspond to the three body reaction with undetected ^{11}C nucleus in the ground state. Besides the peak continuum distribution extending up to Q_3=150 MeV is observed. The excitation of ^{11}C nucleus with practically constant probability to so high excited states is not very likely. Therefore the observed continuous part should be attributed to other reaction mechanism (e.g. four body reaction $\alpha+^{9}Be+p+^{10}B$ which will be discussed later).

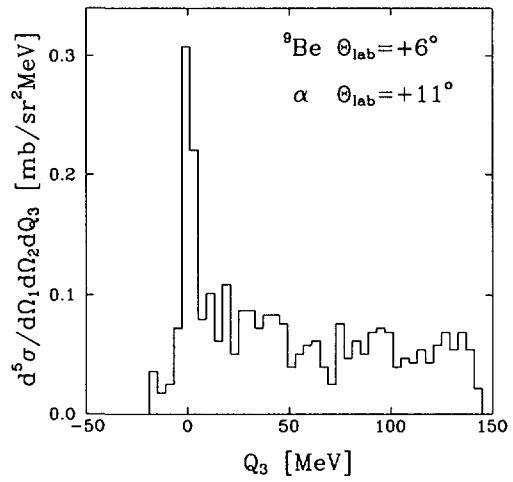

Fig. 21. Experimental coincidence cross section for α–^{9}Be coincidences presented as a function of Q_3.

In case of regarded sequential process the ^{13}C nucleus excited to some states is formed in the intermediate stage of the reaction. Formation of such excited states will manifest itself by concentration of α–^{9}Be coincidence events in peaks at E^*_{12} value corresponding to the excitation energy of $^{13}C^*$ nucleus levels. As examples position of the peaks corresponding to some selected excitation energies E^*_{12} values for α–^{9}Be coincidences for (+6°, +11°) angular configuration are shown in Fig. 19b as points. The excitation of intermediate $^{13}C^*$ levels is well visible when the coincidence cross section is plotted as a function of excitation energy E^*_{12}. It is shown in Fig. 22 where the coincidence spectrum of excitation energy E^*_{12} is presented for α–^{9}Be coincidence events corresponding to the peak at Q_3=0. It is seen from Fig. 22 that following states of ^{13}C nucleus are excited: 11.1, 11.9, 12.3, 12.6, 13.2, 13.9 and 14.4 MeV. Since in that excitation energy range many ^{13}C states exist they cannot be unambiguously assigned to observed peaks. The observation of intermediate ^{13}C

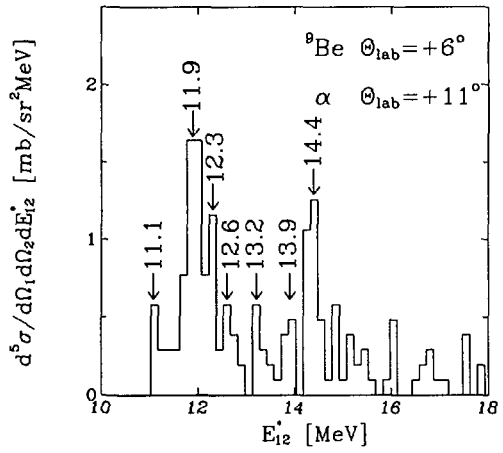

Fig. 22. Experimental coincidence cross section for α–^{9}Be coincidences presented as a function of excitation energy E_{12}^*. Arrows mark the peaks corresponding to the excited states of ^{13}C nucleus, the labels above arrows correspond to values of excitation energy.

states and a peak at Q_3=0 allows the conclusion that sequential reaction initiated by nucleon transfer is in large part responsible for observed α–^{9}Be coincidence cross section.

For (+6°, +11°) angular configuration only the small part of the ^{13}C excitation spectrum may be observed due to small efficiency for large excitation energies. In other angular configurations different part of this excitation spectrum may be observed. In order to compare the excitation probability for various angular configurations the efficiency has to be taken into account. In this way the primary (before decay) distribution of the excitation probability of ^{13}C nucleus may be obtained. The coincidence spectra for α–^{9}Be coincidences corrected for the efficiency at different angular configurations are collected in Fig. 23. It is seen from Fig. 23 that coincidence spectrum depends

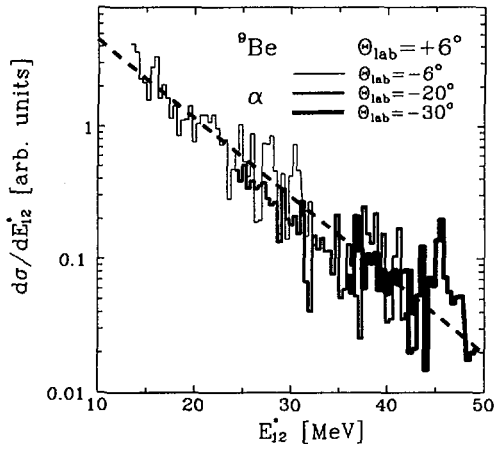

Fig. 23. Experimental coincidence spectra corrected for the efficiency for α–^{9}Be coincidences in different *angular configurations presented as a function of excitation energy* E_{12}^*. *Dashed line corresponds to the* exponential function fitted using the least square method.

exponentially on the excitation energy E^*_{12} and this dependence as well as magnitude of the excitation probability is very similar for different angular configurations. This coincidence spectra corrected for efficiency contain information about formation of intermediate excited states and about probability of their decay into $\alpha+^9$Be channel.

The α–^{9}Be coincidences from decay of ^{13}C nucleus excited to given energy E^*_{12} are observed for some particular angle of primary ^{13}C nucleus (θ_{12cm}) and for specific angles of α particle and ^{9}Be ejectile (θ_{1C} in reference frame of decaying ^{13}C nucleus). This is shown schematically in Fig. 24a. All these angles are different for various excitation energies and angular configurations of detectors as may be seen from Fig. 24b and 24c. When ^{13}C nucleus will be polarized after first stage of reaction its alignment should depend on θ_{12cm} angle. The decay probability of aligned nucleus is described

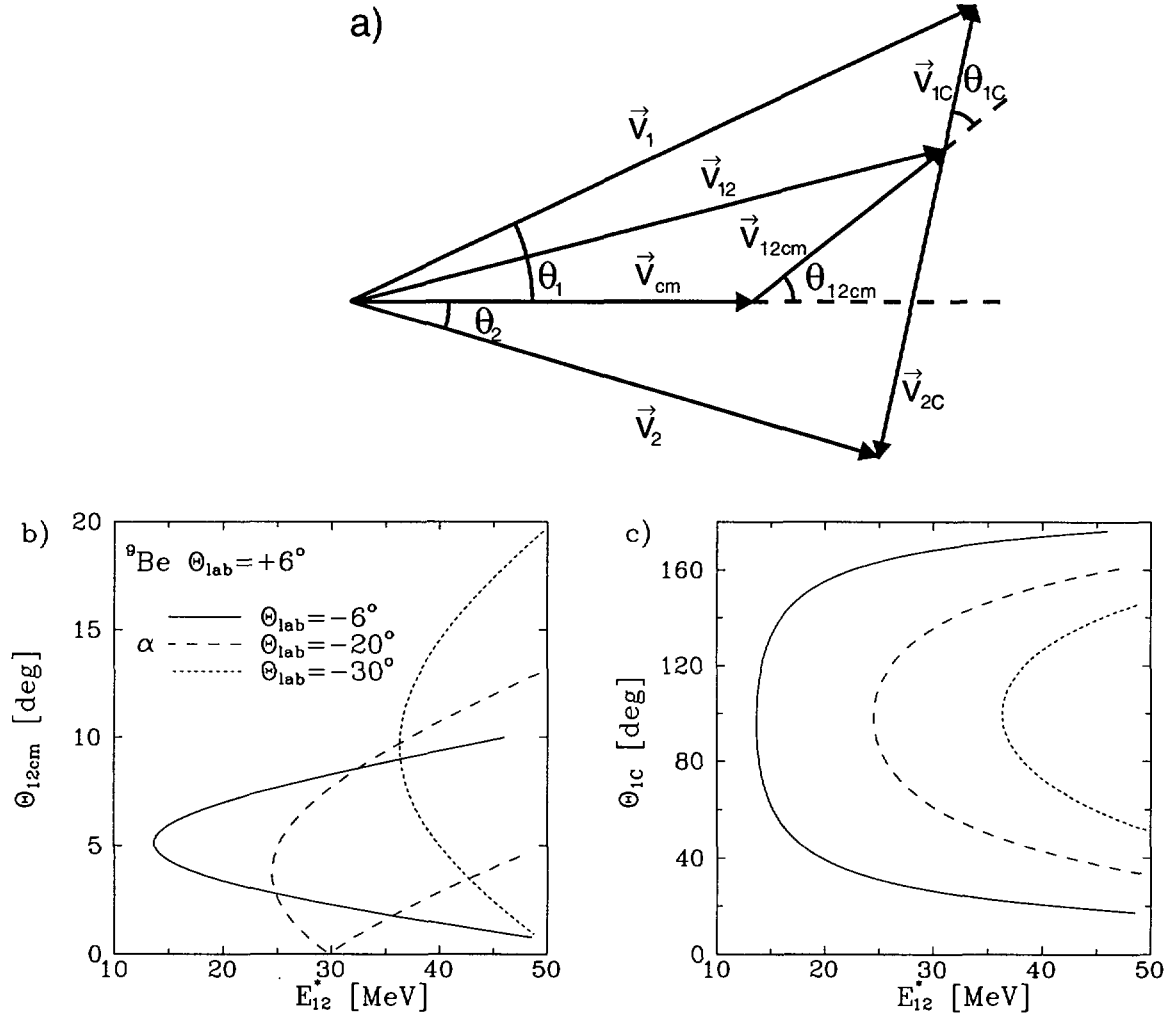

Fig. 24. (a) Velocity vectors of primary ^{13}C nucleus ($\vec{v}_{12}$ – laboratory reference frame and $\vec{v}_{12cm}$ – c.m. reference frame) and the decay products – α particle ($\vec{v}_1$ – laboratory reference frame and $\vec{v}_{1C}$ – reference frame with ^{13}C nucleus at rest) and ^{9}Be nucleus ($\vec{v}_2$ – laboratory reference frame and $\vec{v}_{2C}$ – reference frame with ^{13}C nucleus at rest). The primary ^{13}C nucleus angle in c.m. reference frame (θ_{12cm}), α particle angle (θ_{1C} in reference frame of decaying ^{13}C nucleus) and the detector angles θ_1 and θ_2 are also shown. Dependence of θ_{12cm} angle (b) and θ_{1C} angle (c) on excitation energy E^*_{12} of ^{13}C nucleus.

by correlation function which depend on θ_{1C} angle. Therefore probability of formation and decay of ^{13}C nucleus shown in Fig. 23 should be in principle modulated by some function of these angles different for each excitation energy and angular configuration. However, the smooth dependence of this probability on excitation energy E^*_{12} as well as its weak variation for different angular configuration suggest that in average the alignment of ^{13}C nuclei is not observed. This is equivalent to isotropy of ^{13}C nucleus decay in the reference frame where it is in rest.

Similar coincidence patterns as that for α–^{9}Be coincidences are observed also for α–^{10}B coincidences. As it is seen in Fig. 6 most of coincidence events are concentrated on the kinematical curve for $^{12}C(^{12}C,\alpha^{10}B)^{10}B$ reaction. It indicates that α–^{10}B coincidences in the largest part arise in the three body reaction. In the coincidence spectrum represented in function of E^*_{12} the discrete peaks are visible. It may be seen in Fig. 25, where an example of the α–^{10}B coincidence cross section as a function of E^*_{12} is shown for events corresponding to three body reaction. It is seen that following intermediate ^{14}N nucleus states are observed: 12.2, 12.9, 13.5, 14.1, 14.5, 15.1, 15.6 and 16.3 MeV, which may be identified with known ^{14}N levels. It is therefore deduced that α–^{10}B coincidences may be attributed to the deuteron transfer reaction with excitation of ^{14}N nucleus followed by α particle decay. Also in case of α–^{10}B coincidences the exponential dependence of coincidence spectra corrected for the efficiency on excitation energy E^*_{12} is observed. Just as for α–^{9}Be coincidences this dependence is very similar for all angular configurations, moreover the slope of the spectra is identical with that observed for α–^{9}Be coincidences.

Another type of the coincidence pattern is observed for coincidence of α particles with ^{7}Be, ^{7}Li and ^{6}Li ejectiles. In these cases the coincidence events are concentrated in the region enclosed by appropriate kinematical curve as shown in Fig. 26a for typical example of α–^{6}Li coincidences. They

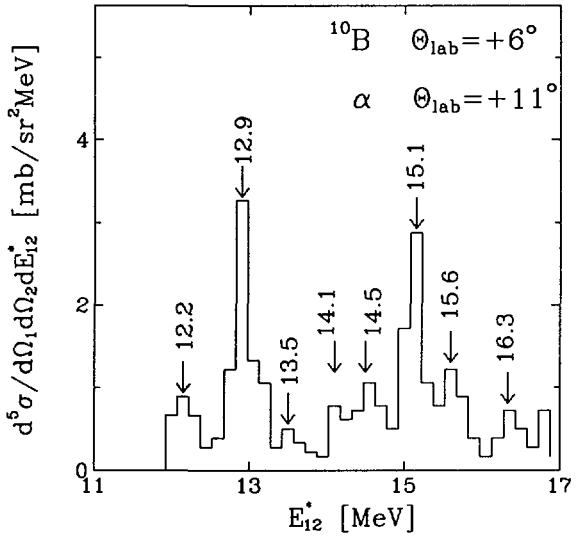

Fig. 25. Experimental coincidence cross section for α–^{10}B coincidences presented as a function of excitation energy E^*_{12}. Arrows mark the peaks corresponding to the excited states of ^{14}N nucleus, the labels above arrows correspond to values of excitation energy.

are not correlated to curves of constant Q_3 value but are grouped on the curves of constant E^*_{12} value as may be seen from comparison of experimental coincidence patterns with curves shown in Fig. 26b. Therefore it may be concluded that more than three body reactions with excitation of intermediate nuclei are responsible for these coincidences. In case of α–^{6}Li coincidences the reactions presented in Fig. 27 may be regarded.

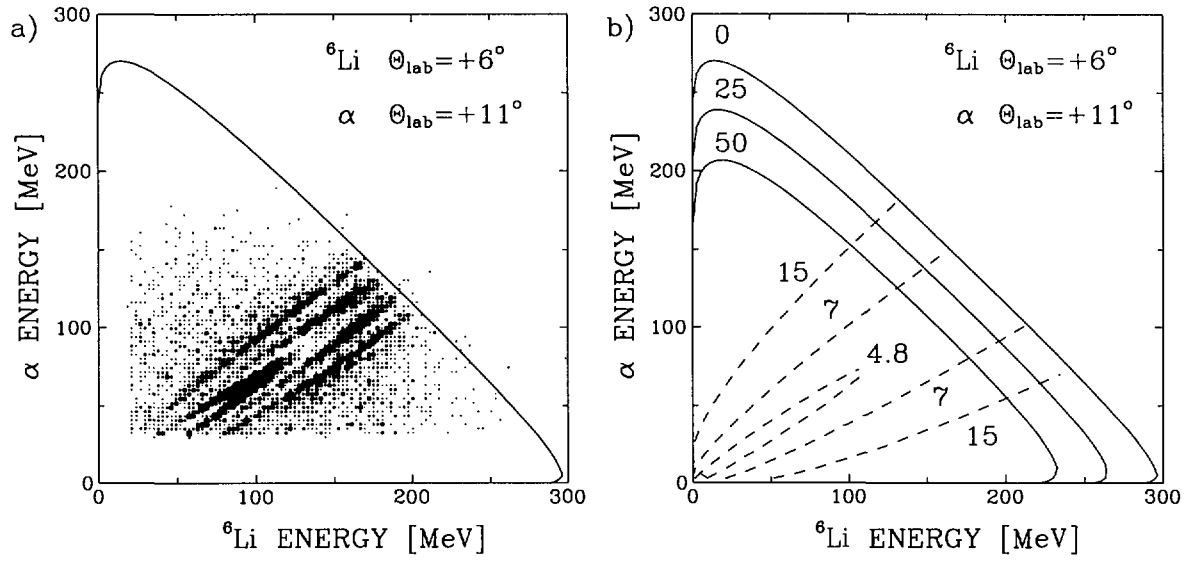

Fig. 26. Two-dimensional spectrum for α–^{6}Li coincidences for angular configuration (+6°,+11°) (a). Solid curve represents the ejectiles energies that correspond to a three body reaction with all final state particles in their ground states (kinematical curve). In part (b) the kinematical curves for various values of missing energy Q_3 (solid lines) and some selected values of excitation energy E^*_{12} (dashed lines). Numbers labeling curves correspond to Q_3 and E^*_{12} values in MeV.

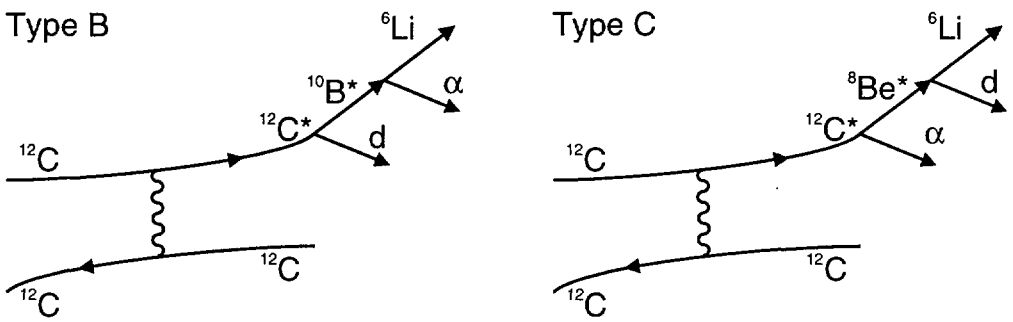

Fig. 27. Schematic representation of inelastic scattering reaction followed by emission of deuteron with formation of intermediate states of ^{10}B nucleus and sequential emission of α particle (Type B) and emission of α particle with formation of intermediate states of ^{8}Be nucleus and sequential emission of deuteron (Type C).

In case of both reactions in the first stage ^{12}C nucleus is excited above the deuteron or α particle decay threshold (25.2 MeV and 7.4 MeV respectively). In process of type B the ^{12}C nucleus decays sequentially emitting deuteron and leaving $^{10}B^*$ nucleus in intermediate excited state which subsequently decays by α particle emission to final ^6Li nucleus. The sequence of $^{12}C^*$ nucleus decays may proceed also in reverse order. In process of type C the excited ^{12}C nucleus emit in the first step α particle producing $^8Be^*$ nucleus in intermediate excited state that further decays emitting deuteron and leaving ^6Li nucleus in a bound state. In case of both decay sequences the different coincidence patterns have to be observed. In case of reaction type B the excitation of intermediate $^{10}B^*$ states should be visible in α–^6Li coincidence spectrum as a concentration of events on curves of constant E^*_{12} value. For reaction of type C α particle and ^6Li are not correlated to some particular relative energy since they do not form intermediate state. Therefore in this case the coincidence events should have continuum distribution. The excitation of ^{10}B levels is well seen in Fig. 28 where the α–^6Li coincidence cross section is presented as function of E^*_{12}. The observed peaks may be identified as corresponding to the following, known from the literature ^{10}B excited states: 4.774 MeV, three states at about 5.1 MeV and group of three states at about 6 MeV. There is no significant continuous contribution observed which should appear in case of sequential process of type C. It suggest that the α–^6Li coincidences are produced mainly in sequential process of type B with deuteron emission in the first decay followed by α particle decay of intermediate ^{10}B nucleus. A strong dumping of the reaction of type C is due to the ^8Be structure which predominantly decays by α particle emission.

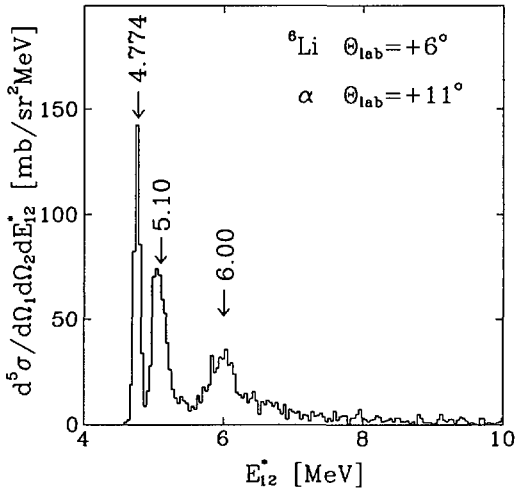

Fig. 28. Experimental coincidence cross section for α–^6Li coincidences presented as a function of excitation energy E^*_{12}. Arrows mark the peaks corresponding to the excited states of ^{10}B nucleus, the labels above arrows correspond to values of excitation energy.

In order to obtain the primary (before decay) excitation energy distribution of ^{10}B nuclei produced in ^{12}C decay after deuteron emission, the experimental α–^6Li coincidence distributions were corrected for the efficiency. The corrected for the efficiency coincidence spectra as a function of

excitation energy E^*_{12} are shown in Fig. 29 for (+6°, –6°) and (+6°, +11°) angular configurations. It is seen that probability for production of intermediate ^{10}B states and their α particle decay decrease exponentially with increasing excitation energy of these states. The shape and the magnitude of this excitation probability are similar for both angular configurations. Similarly as it was discussed for α–^{9}Be coincidences, this fact allows conclusion that ^{10}B decay is in average isotropic in its rest reference frame.

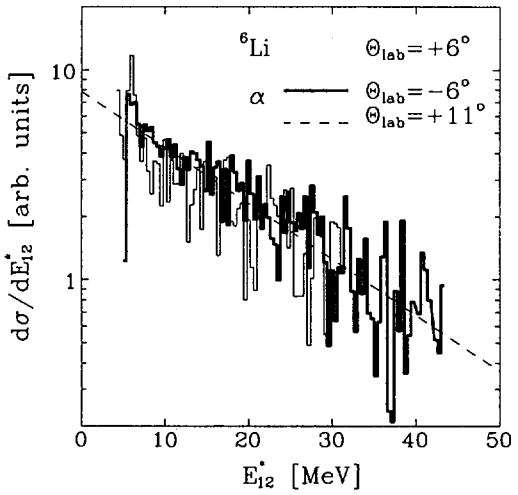

Fig. 29. Experimental coincidence spectra corrected for the efficiency for α–^{6}Li coincidences in different angular configurations presented as a function of excitation energy E^*_{12}. Dashed line corresponds to the exponential function fitted using the least square method.

Similar coincidence patterns with excitation of intermediate states are observed also for α–^{7}Be and α–^{7}Li coincidences. Therefore it may be deduced that similar mechanism as for α–^{6}Li coincidences is responsible for these coincidence cross section. The possible sequential processes leading to α–^{7}Be and α–^{7}Li coincidences are presented in Fig. 30. The ^{12}C nucleus excited in inelastic process decays by neutron or proton emission leading to ^{11}C or ^{11}B excited nuclei. These nuclei subsequently decay emitting α particles which are in coincidence with the decay product ^{7}Be or ^{7}Li nuclei. The decay appearing in reverse order (first α particle emission and next nucleon decay) are

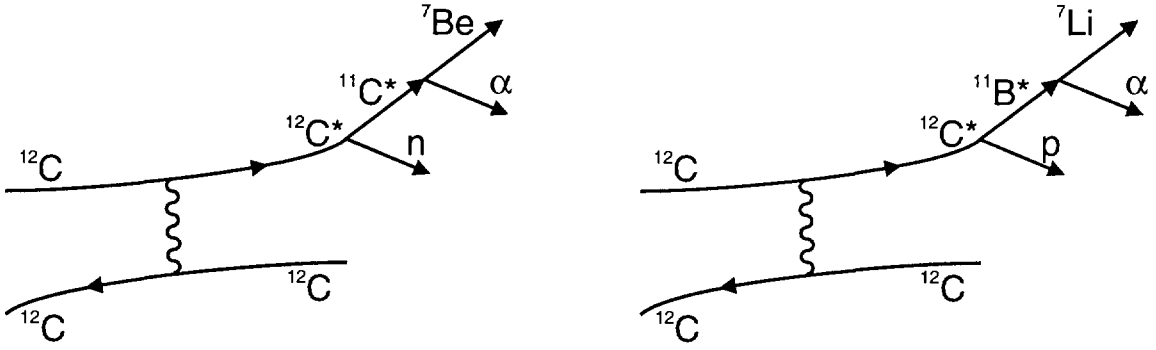

Fig. 30. Schematic representation of inelastic scattering reaction followed by nucleon emission with formation of intermediate ^{11}C and ^{11}B nuclei decaying with α particle emission and leading to ^{7}Be and ^{7}Li final nuclei.

strongly suppressed by ^{8}Be structure which in this case is produced after first decay. The domination of such processes is strongly confirmed by the observation of intermediate excited states in α–^{7}Be and α–^{7}Li coincidence spectra presented in Fig. 31. In case of α–^{7}Be coincidences the excitation of intermediate ^{11}C states of energy 8.1, 8.4 and 8.7 MeV is observed, while for α–^{7}Li coincidences the excited ^{11}B levels of energy 9.1, 10.3 and 11.2 MeV are seen. Exponential dependence of the probability for production and α particle decay of intermediate ^{11}C and ^{11}B nuclei on excitation energy E^{*}_{12} is observed. The slope of α–^{7}Be and α–^{7}Li coincidence spectra corrected for efficiency represented in function of E^{*}_{12} is exactly the same as observed for α–^{6}Li coincidences.

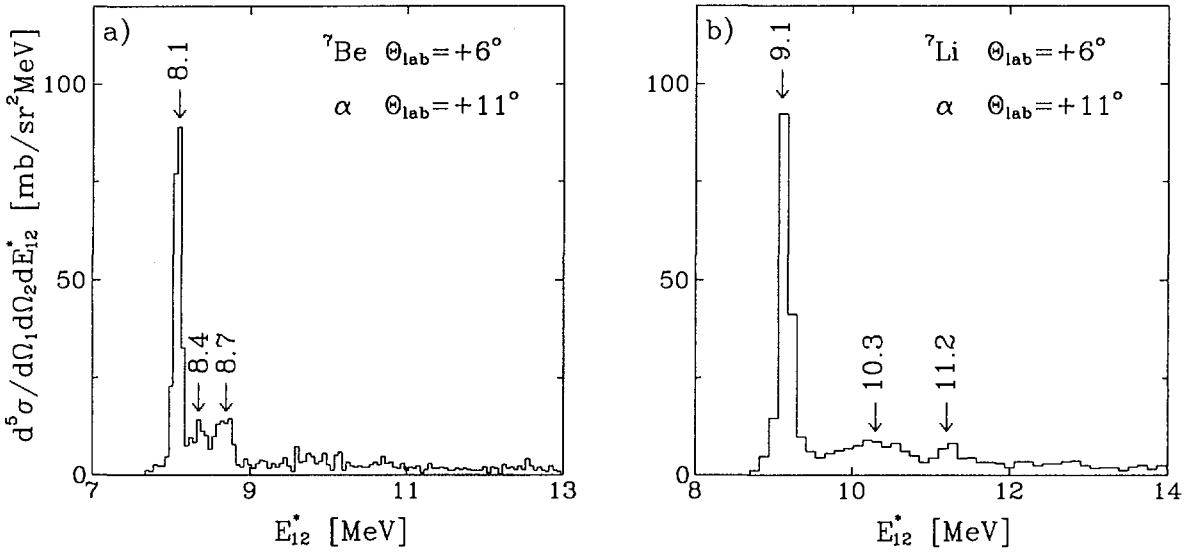

Fig. 31. Experimental coincidence cross section for α–^{7}Be (a) and α–^{7}Li (b) coincidences presented as a function of excitation energy E^{*}_{12}. Arrows mark the peaks corresponding to the excited states of ^{11}C (part a) and ^{11}B (part b) nucleus, the labels above arrows correspond to values of excitation energy.

4.2. α–α coincidences

As a special case the α–α coincidences have to be regarded. The ^{12}C nucleus, due to its three α particle structure, decays predominantly by α particle emission. For excitation energy smaller than 16 MeV only α particle emission is allowed due to the energy threshold for decay with emission of other particles. The decay product – ^{8}Be nucleus is unstable and decays predominantly into two α particles. Thus in the ^{12}C decay three α particles may be produced with large probability. As it was discussed, both projectile and target like nuclei may undergo fragmentation simultaneously. Therefore the interaction of ^{12}C+^{12}C nuclei leads with large probability to six α particles in the exit channel as shown in the diagram in Fig. 32. Any pair of these α particles may be in coincidence.

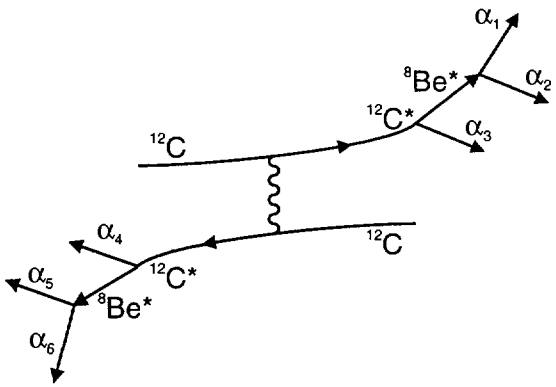

Fig. 32. Schematic representation of inelastic scattering reaction followed by decay of projectile like and target like nucleus into three α particles with formation of intermediate ^{8}Be states.

The example of the α–α coincidence cross section for (+6°, –6°) angular configuration is shown in Fig. 33. It has a maximum at energies corresponding to beam velocity which are marked by arrows. The process of sequential projectile fragmentation leads to α particles with energy distributed close to energy corresponding to the beam velocity. The direct break-up of ^{12}C nucleus into three α particles leads to continuum distribution of α–α coincidence peaked also at such energies. For the coincidence of one α particle from projectile like and one α particle form target like nuclei the coincidence cross section extending up to small particle energies should be observed. The α–α coincidence spectra as a function of E^{*}_{12} corrected for the efficiency are shown in Fig. 34 with marked excitation energy (arrow) and width (bar line over arrow) of ^{8}Be states. For excitation energies smaller than 16 MeV no other ^{8}Be levels are known. Besides the continuum distribution the peak corresponding to 3.04 MeV ^{8}Be state is seen, while the excitation of 11.4 MeV level is not visible. The observed peak correspond to coincidence of α_1–α_2 particles emerging from the decay of excited ^{8}Be nucleus.

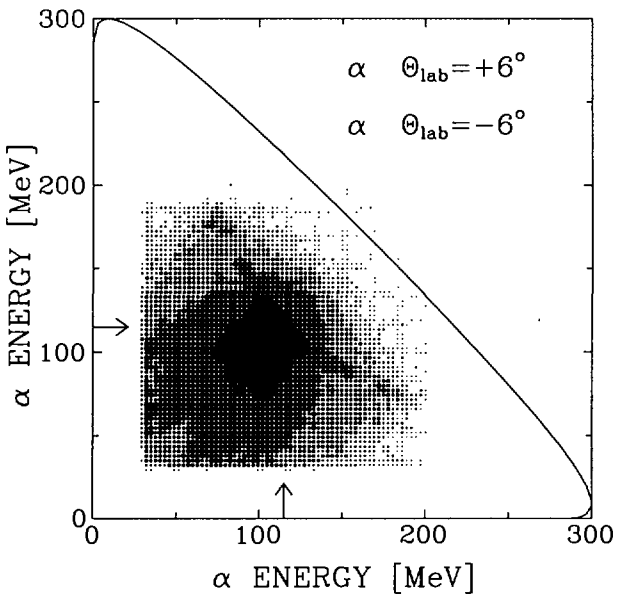

Fig. 33. Two-dimensional spectrum for α–α coincidences for angular configuration (+6°,–6°). Solid curve represents kinematical curve for ^{12}C(^{12}C,αα)^{16}O three body reaction with ^{16}O nucleus in ground state.

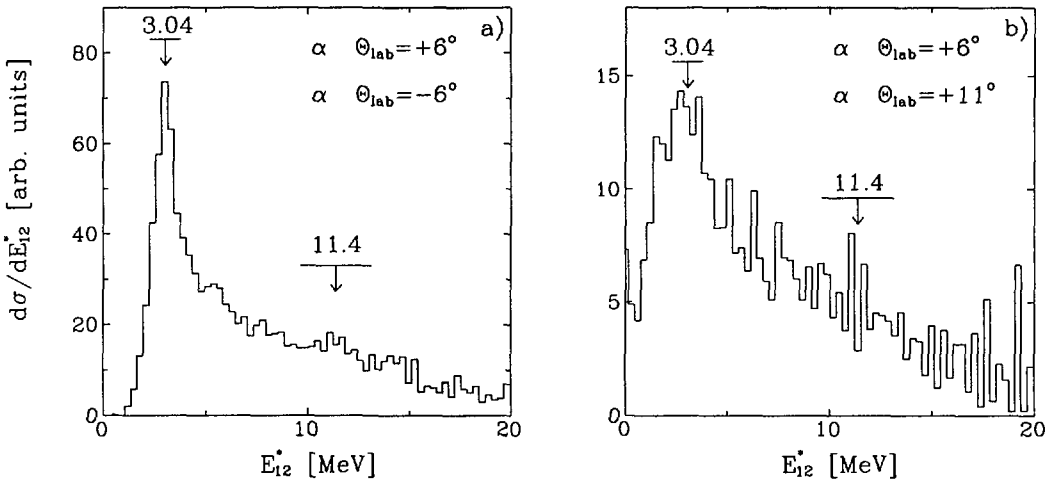

Fig. 34. Experimental coincidence spectra corrected for the efficiency for α–α coincidences for different angular configurations presented as a function of excitation energy E^*_{12}. Arrows with bar line mark position of ^{8}Be excited states with their width.

The coincidences of α_1 and α_2 particles originating from ^{8}Be decay from its ground state cannot be detected. The relative angle of such α particles is very small, therefore they are not in coincidence for investigated angular configurations. Continuum distribution may arise from α_1–α_3 and α_2–α_3 coincidences in case of sequential process. Such coincidences are observed always, independently on that in which state intermediate ^{8}Be is produced. The contribution of prompt projectile fragmentation to the continuum distribution cannot be excluded. The detailed analysis of the relative intensity of the observed peak and continuum distribution should allow estimation of relative probability of formation of intermediate ^{8}Be nuclei in ground and first excited state and possible contribution of prompt fragmentation.

4.3. Results of the model independent analysis

The qualitative, model independent discussion of the kinematical signatures of sequential processes was performed for all measured coincidences. It was shown that observed coincidences may be attributed to the various sequential fragmentation processes. These processes are started either by inelastic excitation or by one or two nucleon transfer reactions. The unbound states excited in these reactions decay in one or two steps. The excitation of intermediate states appearing in the decay chain is visible as the peaks in excitation energy E^*_{12} coincidence spectra. In some cases from the observation of the discrete peaks in the E^*_{12} coincidence spectra it was possible to deduce the sequence in which fragmentation proceeds. Negligible background observed at excitation energies where no intermediate nuclei levels exist suggest that prompt fragmentation may be excluded. Only in case of α–α coincidences the contribution of prompt fragmentation is possible. Smooth dependence of efficiency corrected coincidence spectra on excitation energy shows that in average alignment is not generated in the reaction step proceeding decay. Therefore in average the decay is isotropic in the reference frame of decaying nucleus.

5. Model for sequential process calculations

As it was shown in the previous chapter the direct reactions lead frequently to unbound states which subsequently decay by the particle emission. From the presented qualitative analysis of the coincidence data it follows that most of the observed coincidences may originate from such sequential fragmentation reactions. More quantitative results concerning the sequential processes may be obtained in the frame of the simple model presented in this chapter.

Let us consider the reaction

$$a + b \rightarrow 1 + 2 + ... + n \tag{1}$$

where a denotes projectile, b – target and 1, 2, ... n – ejectiles. The m_i will denote mass, E_i – total energy, $\vec{p_i}$ – momentum and p_i – four momentum of i-th particle (i = a, b, 1, 2, ..., n). The reaction dynamics is described by the transition probability $\wp(\vec{p_a}, \vec{p_b}, \vec{p_1}, \vec{p_2}, ..., \vec{p_n})$ from the initial a + b state to the final state 1 + 2 + ... + n with definite momenta $\vec{p_i}$. The transition probability is determined by the square of the transition amplitude

$$|\langle \vec{p_1}, \vec{p_2}, ..., \vec{p_n}| \hat{A} | \vec{p_a}, \vec{p_b}\rangle|^2 = \wp(\vec{p_a}, \vec{p_b}, \vec{p_1}, \vec{p_2}, ..., \vec{p_n}) \tag{2}$$

where $\hat{A}$ is the operator responsible for the transition. It is a function of the momenta of all incident and outgoing particles. For fixed entrance channel and beam momentum the shorter notation of transition probability in the further formulae will be used:

$$\wp(\vec{p_a}, \vec{p_b}, \vec{p_1}, \vec{p_2}, ..., \vec{p_n}) = \wp(\vec{p_1}, \vec{p_2}, ..., \vec{p_n}) \tag{3}$$

In the inclusive and coincidence experiments only some ejectiles are observed and their momenta are measured. Thus in order to obtain the differential cross sections it is necessary to integrate the square of the transition amplitude over all allowed values of $\vec{p_i}$ of unobserved particles.

The inclusive cross section for observed particle 1 may be represented as

$$2E_1\frac{d^3\sigma_n}{d^3p_1} = \frac{1}{F}\int \prod_{i=2}^{n}\frac{d^3p_i}{2E_i}\,\delta^4(p_a + p_b - p_1 - \sum_{i=2}^{n} p_i)\,\wp(\vec{p_1}, \vec{p_2}, ..., \vec{p_n}) \tag{4}$$

and a coincidence cross section for observed particles 1 and 2 as

$$4E_1E_2\frac{d^6\sigma_n}{d^3p_1d^3p_2} = \frac{1}{F}\int \prod_{i=3}^{n}\frac{d^3p_i}{2E_i}\,\delta^4(p_a + p_b - p_1 - p_2 - \sum_{i=3}^{n} p_i)\,\wp(\vec{p_1}, \vec{p_2}, ..., \vec{p_n}) \tag{5}$$

with the four momentum conservation introduced by δ-function, the $\frac{d^3p_i}{2E_i}$ is the phase space density for particle i. Normalization factor $F = 4\, m_b^2\, |\vec{p}_{a_{lab}}|\, (2\pi)^{3n-4}$ corresponds to the flux of the incident particles, $\vec{p}_{a_{lab}}$ being the beam momentum in the laboratory system.

Using these expressions the inclusive cross sections and the two particle coincidence cross sections, as a function of laboratory kinetic energy (T_1 and T_2) and laboratory solid angle (Ω_1 and Ω_2) as measured experimentally, may be calculated using the jacobian of the transformation

$$dT_i d\Omega_i = \frac{d^3p_i}{|\vec{p_i}|\, E_i}$$

$$\frac{d^3\sigma}{dT_1 d\Omega_1} = |\vec{p_1}|\, E_1 \frac{d^3\sigma}{d^3p_1} \tag{6}$$

$$\frac{d^6\sigma}{dT_1 d\Omega_1 dT_2 d\Omega_2} = |\vec{p_1}|\, |\vec{p_2}|\, E_1\, E_2 \frac{d^6\sigma}{d^3p_1 d^3p_2} \tag{7}$$

5.1. Formulation of the model

The unbound states excited in the direct reactions (inelastic excitation, transfer processes) may decay by particle emission leading to nuclei in bound states (what corresponds to three body exit channels) or in unbound states which subsequently decay by particle emission (it corresponds to four, five or more body exit channels). Such processes are presented schematically in Fig. 35. In the first stage of the reaction two nuclei are produced: projectile like nucleus (moving approximately in the beam direction with the beam velocity) and target like nucleus – n (with very small energy in the laboratory reference frame). In the further steps of reaction excited projectile like nucleus decays emitting various particles – 1, 2, ..., n–2.

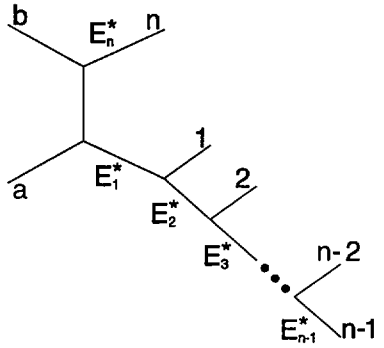

Fig. 35. Schematic representation of n body sequential process.

In order to analyse such processes the square of the transition amplitude $\wp(\vec{p}_1, \vec{p}_2, \ldots, \vec{p}_n)$ is needed. It is assumed that for the regarded sequential processes the formation of excited nuclei and their decay are well separated in time. This separation is long enough that it may be assumed that all formation and decay processes are independent. Under this assumption the transition probability may be factorized and represented as a product of probabilities $\wp_1$, $\wp_2$, ..., $\wp_{n-1}$. The $\wp_1$ describes the transition probability in the first step of reaction (direct process) and $\wp_2$, ..., $\wp_{n-1}$ describe decay probabilities in successive decays. For unpolarized particles in the entrance and exit channels $\wp_1$ is a function of three variables only (e.g. the center of mass polar angle of the projectile like nucleus and the excitation energy of the projectile and target like nuclei). The decay probabilities are in general the function of the primary excitation energy (before decay), final excitation energy of the

decay products, and the emission angles of the decay products measured in the reference frame of the decaying nucleus. The angular dependence appears when the decaying nuclei are polarized. In the present analysis the polarization effects were not taken into account. In the excitation energy region where unbound states occur many levels with various spin are excited. It may be expected that at such energies alignment of nuclei averaged over excitation energy equals zero. This averaging leads finally to angle independent decay probability what is equivalent to the assumption that all decays are isotropic in the rest frame of the decaying nucleus. This assumption is confirmed by the smooth dependence of coincidence spectra on the excitation energy of intermediate nuclei (see section 4.1).

Finally the transition probability used in the analysis has the form

$$\wp(\vec{p_1}, \vec{p_2}, \ldots, \vec{p_n}) = \wp_1(\theta_{cm}, E_1^*, E_n^*)\, \wp_2(E_1^*, E_2^*) \ldots \wp_{n-1}(E_{n-2}^*, E_{n-1}^*) \qquad (8)$$

where θ_{cm} is the centre of mass angle of projectile like fragment produced in the first step of reaction, E_1^* is the excitation energy of the projectile like fragment that subsequently decays, E_n^* is the excitation energy of target like nucleus, $E_2^*, \ldots, E_{n-1}^*$ are the excitation energies of fragments produced in subsequent decays. Since the time separation of each reaction step was assumed, the possible decay of the target like nuclei does not influence the processes of projectile like nuclei decay. Therefore regarding projectile like nuclei fragmentation it is not necessary to take into account the target like nuclei fragmentation (or vice versa). Only for coincidences of one particle originating from projectile like nucleus and second from target like fragment it is necessary to regard simultaneous decay of projectile and target like nuclei.

The phenomenological analysis was performed using parameterization of transitions probabilities $\wp_1, \wp_2, \ldots, \wp_{n-1}$. The experimental angular distributions for inelastic and transfer reactions leading to discrete states of final nuclei exhibit exponential dependence on the centre of mass angle (Fig. 5). Also the theoretical angular distributions for direct processes have exponential form. Therefore the angular dependence of amplitude $\wp_1$ was assumed in the form of the exponential function of the centre of mass angle θ_{cm} of projectile like fragment. From the model independent analysis of the coincidence data for three body reaction (presented in Fig. 23) it follows that also the dependence of the transition probability on excitation energy E_1^* have the exponential form. The dependence of the transition probability on target like nucleus excitation energy E_n^* was assumed to have also exponential form. Similar analysis of four body reactions (presented in Fig. 29) leads to the conclusion that transition probability depends exponentially on excitation energy E_2^* of formed intermediate states. Exponential dependence of transition probability on excitation energies $E_3^*, \ldots, E_{n-1}^*$ of subsequent intermediate states was also assumed. Under these assumptions the transition probability $\wp$ may be written finally as:

$$\wp(\vec{p_1}, \vec{p_2}, \ldots, \vec{p_n}) = N\, e^{-\beta\theta_{cm}}\, e^{-\gamma E_1^*}\, e^{-\delta E_2^*} \ldots e^{-\varepsilon E_{n-1}^*}\, e^{-\zeta E_n^*} \qquad (9)$$

where N is the normalization factor that has to be adjusted to describe the absolute value of the experimental cross section. The parameters $\gamma, \delta, \ldots, \varepsilon$ and ζ are treated as free parameters that have

to be adapted to describe experimental energy spectra. These parameters contain both probability of formation and decay of the excited states. In this way these two processes cannot be distinguished in the phenomenological analysis. Due to this the parameters may be different for each sequential fragmentation process.

In the present analysis the excitation and subsequent decay of both projectile and target like nuclei were regarded. For the identical particles in the entrance channel it may be done very easily since the probability of excitation of projectile and target like nuclei is exactly the same. Therefore it is not necessary to introduce any additional parameters but is enough to use fore-aft symmetry of the transition probability. It was done by taking the sum of transition probabilities $\wp$ given by (9) for centre of mass angles θ_{cm} and $\pi-\theta_{cm}$. In this way transition probability used in the calculations has finally the form:

$$\wp(\vec{p1}, \vec{p2}, \ldots, \vec{pn}) = N\left(e^{-\beta\theta_{cm}} + e^{-\beta(\pi-\theta_{cm})}\right) e^{-\gamma E_1^*} e^{-\delta E_2^*} \ldots e^{-\varepsilon E_{n-1}^*} e^{-\zeta E_n^*} \qquad (10)$$

The addition of transition probabilities (not the transition amplitudes) neglects the interference term, which may be important for specific energies and angles when transition amplitudes for projectile and target like nuclei excitations become comparable.

5.2. Parameters used in the analysis

According to the formula (10) the parameters necessary in the calculations of sequential processes are: primary angular distribution parameter β, parameters γ and ζ describing primary excitation energy dependence of formation and decay of projectile and target like nuclei, respectively, and the normalization factor N. In case when the decay proceeds in two or more steps additional parameters δ, ε etc. describing formation and decay of intermediate excited states have to be known. Values of parameters γ, δ, ε, ... may be different for each sequential process since they describe production of different nuclei and their decay into various channels. It was found, however, that good description of the experimental data may be obtained with fixed values of parameters. Therefore instead of adjusting magnitude of these parameters separately for each process, the values presented below were used.

Value of parameter β describing primary angular distribution was deduced from experimental and theoretical angular distributions for direct processes. In the performed analysis parameter β was kept constant and had a value of 0.15 $1/_{deg}$ as obtained from theoretical DWBA angular distributions at excitation energies in the region of unbound states.

In the analysis of sequential processes initiated by nucleon and deuteron transfer parameter $\gamma_{trans.} = 0.13\ 1/_{MeV}$ describing formation and decay of projectile like nuclei was used. This value was obtained from the experimental coincidence spectra for three body reactions leading to α–^{9}Be and α–^{10}B coincidences (Fig. 23). In case of transfer reactions the excitation of target like nuclei was not considered. This assumption is confirmed by observation of the strong peak at Q_3=0 (three body reaction with all final state particles in ground state) in α–^{10}B and α–^{9}Be coincidence spectra (Fig. 21).

The sequential processes started by inelastic excitation were analysed with parameters $\gamma_{inel.} = \zeta_{inel.} = 0.04$ 1/MeV. They should be equal for identical projectile and target nuclei. This value was adopted from the analysis of α particle and ^{12}C ejectile distributions. The details of this analysis will be presented in next chapter.

For processes in which decay occurs in two or more steps values of parameters $\delta = \varepsilon = ... = 0.06$ 1/MeV were used. They were fixed according to the dependence of the experimental coincidence cross section on excitation energy (Fig. 29) for four body reactions leading to α–^{7}Be, α–^{7}Li and α–^{6}Li coincidences.

The normalization factor N was adjusted in order to reproduce the experimental inclusive and coincidence data. Using obtained normalization factor N the total cross section for each analysed sequential process may be calculated by integration of the calculated distributions (equation 6) over solid angle and energy of outgoing particle.

The choice of values of parameters β, γ, δ, ... used in the calculations was not very critical for the results of the analysis. E.g. variation of $\gamma_{inel.}$ parameter (for sequential processes started by inelastic excitation) in 0.03–0.05 1/MeV range as well as β parameter in 0.1–0.2 1/deg range leads to very similar description of the experimental data. The results of the calculations are not very sensitive on values of parameters therefore the cross sections for various sequential processes resulting from the analysis were estimated with an error of about 15%.

6. Analysis of the sequential processes

The importance of sequential fragmentation processes in the $^{12}C+^{12}C$ interaction was shown in the model independent analysis of coincidence data presented in chapter 4. In this section a quantitative analysis will be presented. It was performed by means of sequential fragmentation model formulated in the previous chapter. The inclusive and coincidence spectra were calculated according to formulae (4) and (5), respectively, with the transition probability given by formula (10). The parameters of the transition probability have values given in section 5.2. The only free parameter – normalization factor was varied in order to reproduce the magnitude of experimental cross sections. The example of the sequential processes analysis will be discussed in details for outgoing ^{9}Be and ^{6}Li nuclei and α particles. The energy spectra of ^{12}C nuclei accompanying fragmentation processes will be also presented.

6.1. ^{9}Be inclusive spectra and α–^{9}Be coincidences

As it was shown in chapter 4 many of the observed α–^{9}Be coincidences arise in the sequential reaction started by neutron transfer (Fig. 20). The calculations for such reaction were performed using parameter $\gamma_{trans.} = 0.13$ 1/MeV obtained from the coincidence spectra (Fig. 23). The only free parameter, the normalization factor that was adjusted in order to reproduce α–^{9}Be coincidence data corresponding to three body reaction $^{12}C(^{12}C,\alpha^{9}Be)^{11}C$, i.e. for events belonging to the peak at $Q_3=0$ (Fig. 21). The results of these calculations are shown in Fig. 36 (dashed line) together with the experimental coincidence spectra for events concentrated on the kinematical curve for $\alpha+^{9}Be+^{11}C$ three body reaction (see e.g. Fig. 19a). Besides α–^{9}Be coincidence events corresponding to discussed three body process, the coincidences with large missing energy Q_3 are observed (Fig. 21). They may be attributed to more than three body reaction, e.g. deuteron transfer reaction followed by proton and α particle emission $^{12}C+^{12}C \rightarrow \alpha+^{9}Be+p+^{10}B$. The calculations for such sequential reaction were performed using parameters $\gamma_{trans.} = 0.13$ 1/MeV and $\delta = 0.06$ 1/MeV. The normalization factor was fitted in order to reproduce α–^{9}Be coincidence energy spectra for events not belonging to peak at $Q_3 = 0$. The results of these calculations are compared with the experimental coincidence spectra in Fig. 37 (thin solid line). The coincidence spectra obtained from compound nucleus analysis are also shown in Fig. 37 (thin dashed line). The sum of the cross section for regarded sequential reactions and that resulting from compound nucleus calculations (thick solid line in Fig. 37) very well reproduce experimental coincidence data.

Using the same values of parameters $\gamma_{trans.}$ and δ as well as the normalization factors N the calculations of the inclusive cross section for outgoing ^{9}Be were performed. Their results are shown in Fig. 38 as a thick solid line together with experimental cross section for ^{9}Be ejectiles for various laboratory angles. It is seen that these processes account entirely for experimental cross section at large emission angles, while the experimental cross section at small angles is not reproduced. Another possible process leading to outgoing ^{9}Be nuclei is the inelastic excitation of ^{12}C nuclei with subsequent decay into $^{3}He+^{9}Be$. The calculations for such process were performed with parameters $\gamma_{inel.} = \zeta_{inel.} = 0.04$ 1/MeV and the normalization factor N for this process was adjusted in order to fit

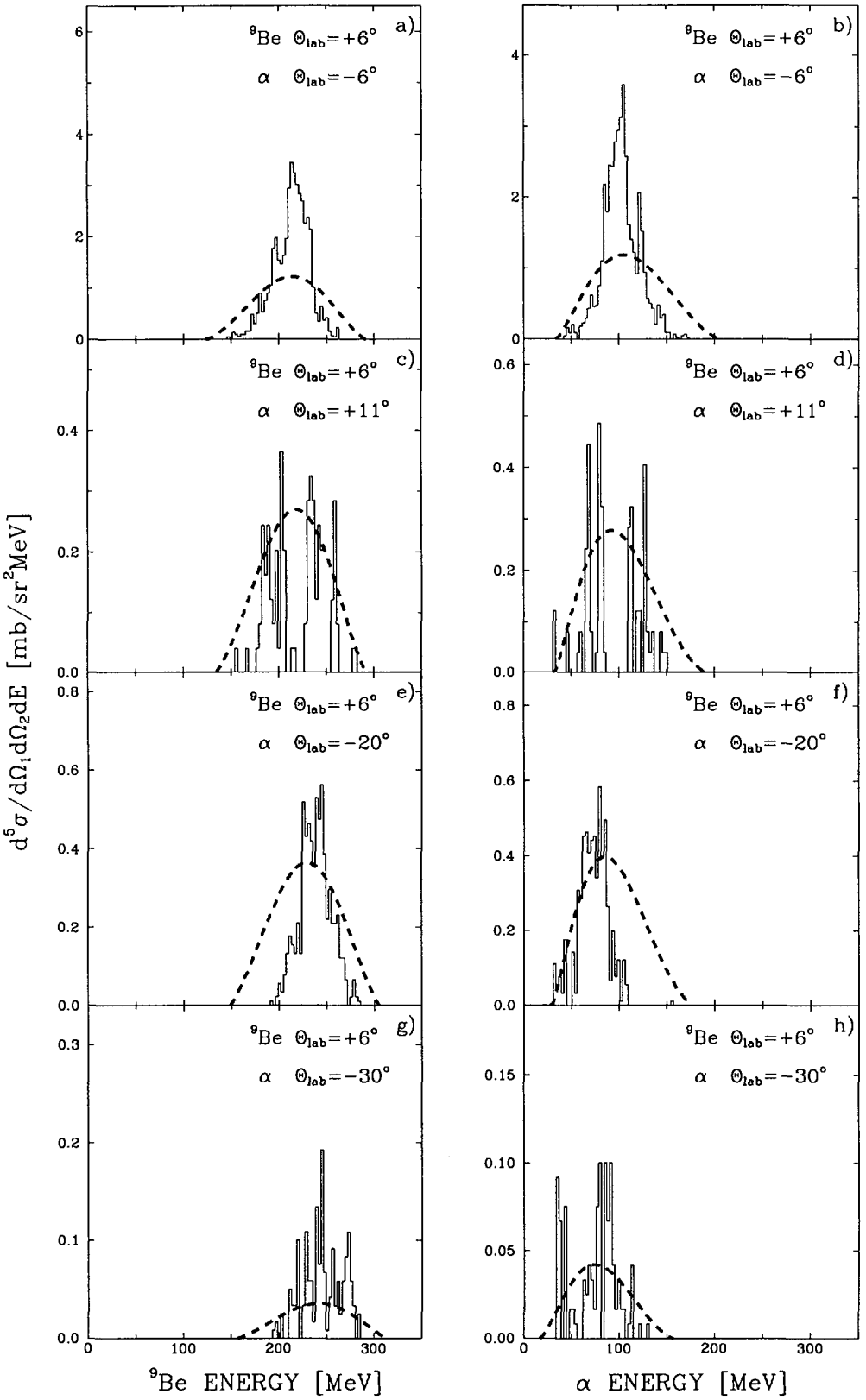

Fig. 36. Experimental α–^{9}Be coincidence spectra corresponding to ^{12}C(^{12}C,α^{9}Be)^{11}C three body reaction (only events concentrated on kinematical curve α+^{9}Be+^{11}C) compared with the sequential fragmentation process calculations (dashed lines).

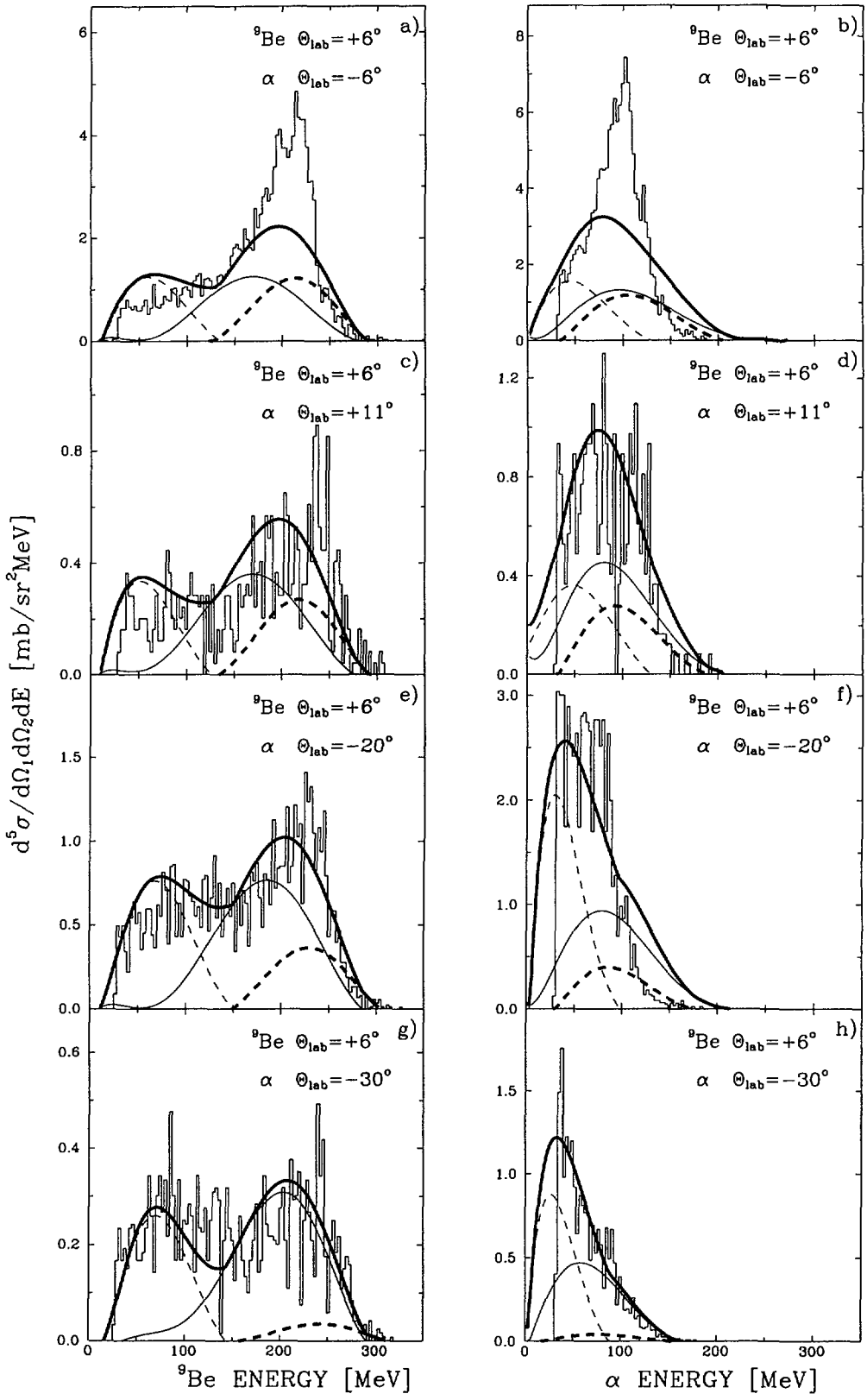

Fig. 37. Experimental α–^{9}Be coincidence spectra compared with sequential processes calculations (α+^{9}Be+^{11}C – thick dashed lines and α+^{9}Be+p+^{10}B – thin solid lines), compound nucleus calculations – thin dashed lines and sum of all these processes – thick solid lines.

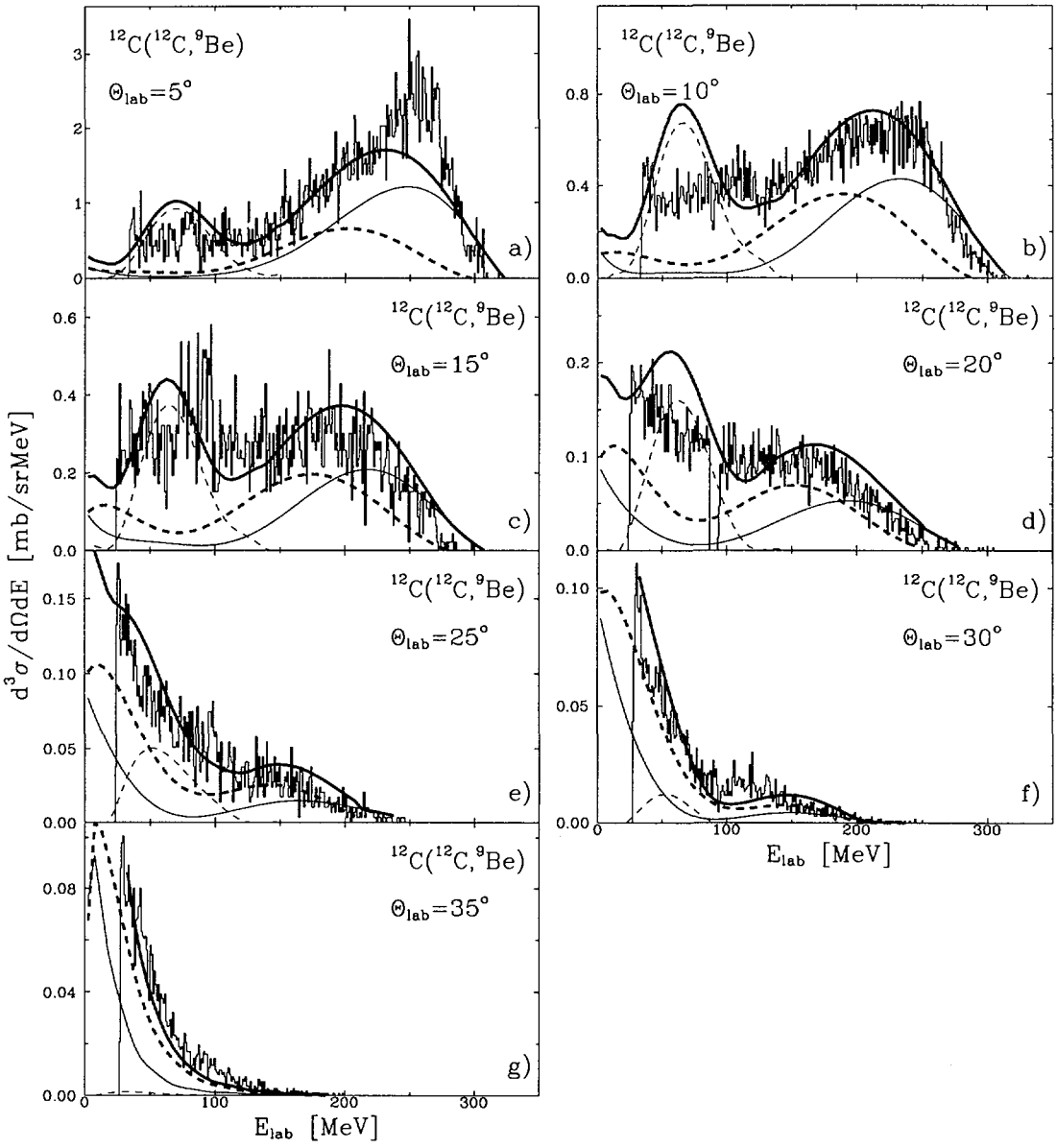

Fig. 38. Experimental ^{9}Be inclusive spectra for various laboratory angles compared with the calculations. Thin solid lines correspond to sequential process leading to $^{3}He+^{9}Be+^{12}C$, thick dashed lines correspond to sum of sequential processes leading to $\alpha+^{9}Be+^{11}C$ and $\alpha+^{9}Be+p+^{10}B$, thin dashed lines – compound nucleus calculations, solid lines represent sum of these sequential processes and results of compound nucleus calculations.

the experimental cross section at small laboratory angles. The results of the calculations are shown in Fig. 38 as thin solid line. It is visible that for small laboratory angles this process leads to the cross section concentrated in a bump at large ejectile energies, while at large angles the contribution of these process to the experimental cross section is small. In Fig. 38 the sum of the cross section for described above sequential processes as well as the cross section for ^{9}Be produced as the evaporation residuum is shown as the thick solid line. It is seen that experimental spectra in a broad angular range are well reproduced by the calculations. Total cross sections for regarded sequential fragmentation processes resulting from the analysis are presented in Table 1.

Table 1. The decay channels taken into account in the calculations of the sequential processes started by inelastic excitation and one and two nucleon transfer processes. The total cross section resulting from the comparison of the calculations with experimental data is also shown for each regarded process.

Primary nucleus	Decay channel	σ_{tot} [mb]
^{12}C	$^{12}C \rightarrow n + {}^{11}C$	37
	$^{12}C \rightarrow p + {}^{11}B$	52
	$^{12}C \rightarrow d + {}^{10}B$	55
	$^{12}C \rightarrow \begin{cases} n + {}^{11}C \rightarrow n + p + {}^{10}B \\ p + {}^{11}B \rightarrow p + n + {}^{10}B \end{cases}$	38
	$^{12}C \rightarrow {}^{3}He + {}^{9}Be$	16
	$^{12}C \rightarrow n + {}^{11}C \rightarrow n + \alpha + {}^{7}Be$	44
	$^{12}C \rightarrow p + {}^{11}B \rightarrow p + \alpha + {}^{7}Li$	50
	$^{12}C \rightarrow d + {}^{10}B \rightarrow d + \alpha + {}^{6}Li$	53
	$^{12}C \rightarrow \begin{cases} n + {}^{11}C \rightarrow n + p + {}^{10}B \\ p + {}^{11}B \rightarrow p + n + {}^{10}B \end{cases} \rightarrow n + p + \alpha + {}^{6}Li$	43
	$^{12}C \rightarrow \alpha + {}^{8}Be \rightarrow \alpha + \alpha + \alpha$	392
^{13}C ^{13}N	$^{13}C \rightarrow n + {}^{12}C \rightarrow n + n + {}^{11}C$ $^{13}N \rightarrow p + {}^{12}C \rightarrow p + n + {}^{11}C$	26
	$^{13}C \rightarrow n + {}^{12}C \rightarrow n + p + {}^{11}B$ $^{13}N \rightarrow p + {}^{12}C \rightarrow p + p + {}^{11}B$	43
	$^{13}C \rightarrow \alpha + {}^{9}Be$	3
	$^{13}C \rightarrow n + n + {}^{11}C \rightarrow n + n + \alpha + {}^{7}Be$ $^{13}N \rightarrow n + p + {}^{11}C \rightarrow n + p + \alpha + {}^{7}Be$	16
	$^{13}C \rightarrow n + p + {}^{11}B \rightarrow n + p + \alpha + {}^{7}Li$ $^{13}N \rightarrow p + p + {}^{11}B \rightarrow p + p + \alpha + {}^{7}Li$	23
^{14}N	$^{14}N \rightarrow \alpha + {}^{10}B$	3
	$^{14}N \rightarrow p + {}^{13}C \rightarrow p + \alpha + {}^{9}Be$	17

6.2. ^{6}Li inclusive spectra and α–^{6}Li coincidences

In the previous section it was shown that ^{6}Li is produced in the sequential process initiated by inelastic excitation of ^{12}C nucleus followed by decay chain $^{12}C^{*} \rightarrow {}^{10}B^{*}+d \rightarrow {}^{6}Li+\alpha+d$ (process B in Fig. 27). The calculations of inclusive ^{6}Li spectra as well as α–^{6}Li coincidence spectra were performed for such sequential process (with parameters $\gamma_{inel.} = 0.04$ 1/MeV and $\delta = 0.06$ 1/MeV). The normalization factor was adjusted in order to fit high energy part of coincidence experimental spectra for "close geometry" configurations. The results of calculations (thick dashed line) are compared with the experimental data in Fig. 39 for ^{6}Li inclusive spectra and in Fig. 40 for α–^{6}Li coincidences. It is seen that the cross section obtained for regarded process contributes significantly to the inclusive

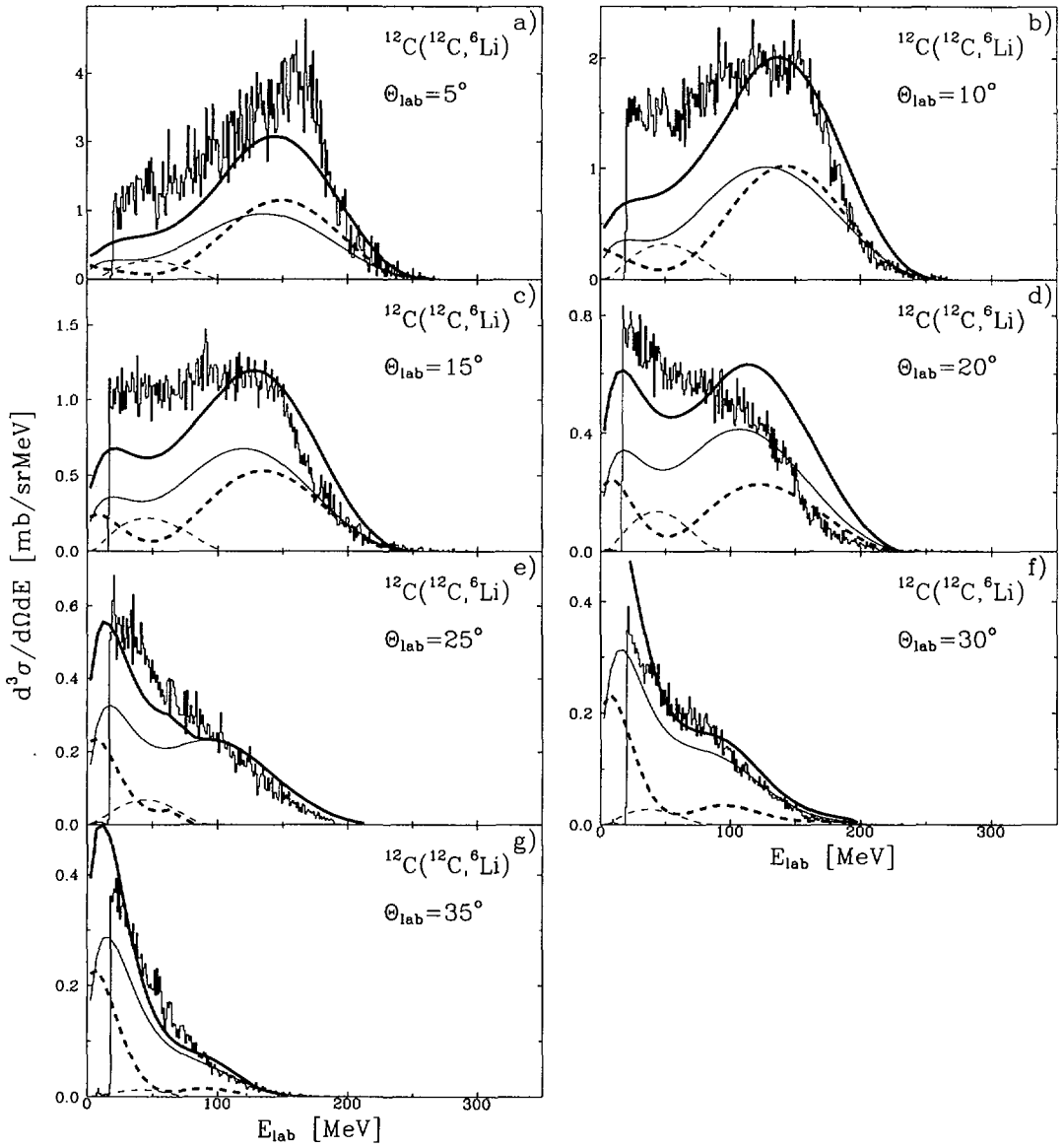

Fig. 39. Experimental ^{6}Li inclusive spectra for various laboratory angles compared with the calculations. Thick dashed lines – sequential process leading to $\alpha+{}^{6}Li+d+{}^{12}C$, thin solid lines – sequential process leading to $\alpha+{}^{6}Li+n+p+{}^{12}C$, thin dashed lines – compound nucleus calculations and thick solid lines – sum of all these processes.

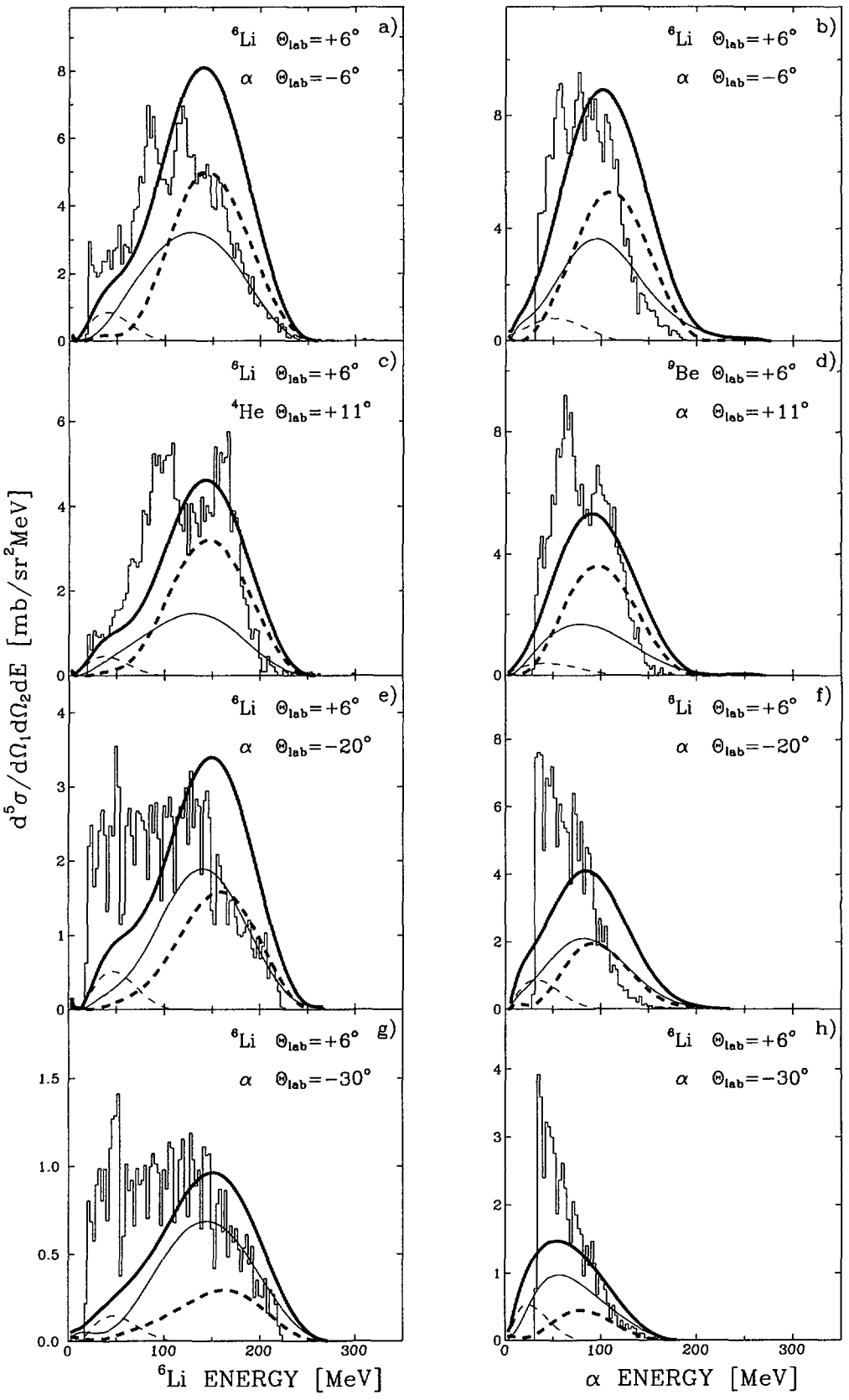

Fig. 40. Experimental α–^{6}Li coincidence spectra compared with calculations of various processes. For description of different lines see Fig. 39.

spectra. At large ^{6}Li laboratory angles this process gives small contribution to the experimental cross section. Therefore sequential process with inelastic excitation of ^{12}C nuclei followed by the decay to n+p+α+^{6}Li final state was considered. The spectra calculated for this process (with parameters $\gamma_{inel.} = 0.04$ 1/MeV and $\delta = \varepsilon = 0.06$ 1/MeV) were normalized in order to describe the experimental inclusive spectra at large angles. The results of the calculations for this process are shown in Fig. 39 and 40 as thin solid line. The distributions obtained from compound nucleus analysis are also shown in Fig. 39 and 40 as thin dashed line. It is seen that sum of all these processes (sequential and compound nucleus reactions) plotted as thick solid line reasonably well reproduce coincidence data for all investigated angular configurations and the inclusive spectra in whole measured angular range. Total cross sections for the regarded sequential processes obtained from the analysis are presented in Table 1.

6.3. Results for other ejectiles

The inclusive and coincidence spectra for other ejectiles were also analysed in the same manner in frame of sequential fragmentation model. The sequential processes presented in Table 1 leading to final ^{11}C, ^{11}B, ^{10}B, ^{7}Be and ^{7}Li nuclei were taken into account. The results of the calculations for these ejectiles are shown in Fig. 41 (thick dashed line) together with experimental inclusive spectra for laboratory angle $\theta_{lab}=5^{o}$. Similarly good description was obtained in the whole measured angular range. The evaporation residua cross section obtained from compound nucleus analysis is also shown in Fig. 41 as thin dashed line. It is seen that sequential fragmentation processes account for large part of experimental cross section and together with cross section from compound nucleus calculations describe very well experimental spectra (solid line in Fig. 41). Part of the ^{11}C and ^{11}B spectra at high energies not reproduced by sequential processes corresponds to one nucleon transfer reactions discussed in section 3.4. A small contribution of deuteron transfer reaction is also seen in high energy part of ^{10}B spectrum. Total cross sections for each sequential process derived from the analysis are also given in Table 1.

6.4. α particle inclusive spectra and α–α coincidences

In some of the regarded above sequential processes α particles are emitted (see Table 1). They contribute to the measured inclusive α particle spectra. In order to find this contribution the inclusive cross section of α particles associated with ^{9}Be, ^{7}Be, ^{7}Li and ^{6}Li ejectiles was calculated using sequential fragmentation model. The parameters (including normalization factor) used in the calculations were the same as in the analysis of ^{9}Be, ^{7}Be, ^{7}Li and ^{6}Li nuclei distributions. The results of the calculations are shown in Fig. 42 (thick dashed line) together with experimental α particle spectra. It is visible that the contribution of these processes to production of α particles is rather small.

The main source of α particles produced in ^{12}C+^{12}C interaction is inelastic excitation of ^{12}C nuclei (target, projectile or mutual target and projectile) above the α particle decay threshold. This is confirmed by very well description of α particle spectra by results of classical dynamical α–cluster model applied to the investigated reaction[100]. From α–α coincidences it follows that ^{12}C nucleus decay into three α particles proceeds sequentially with production of intermediate ^{8}Be nucleus.

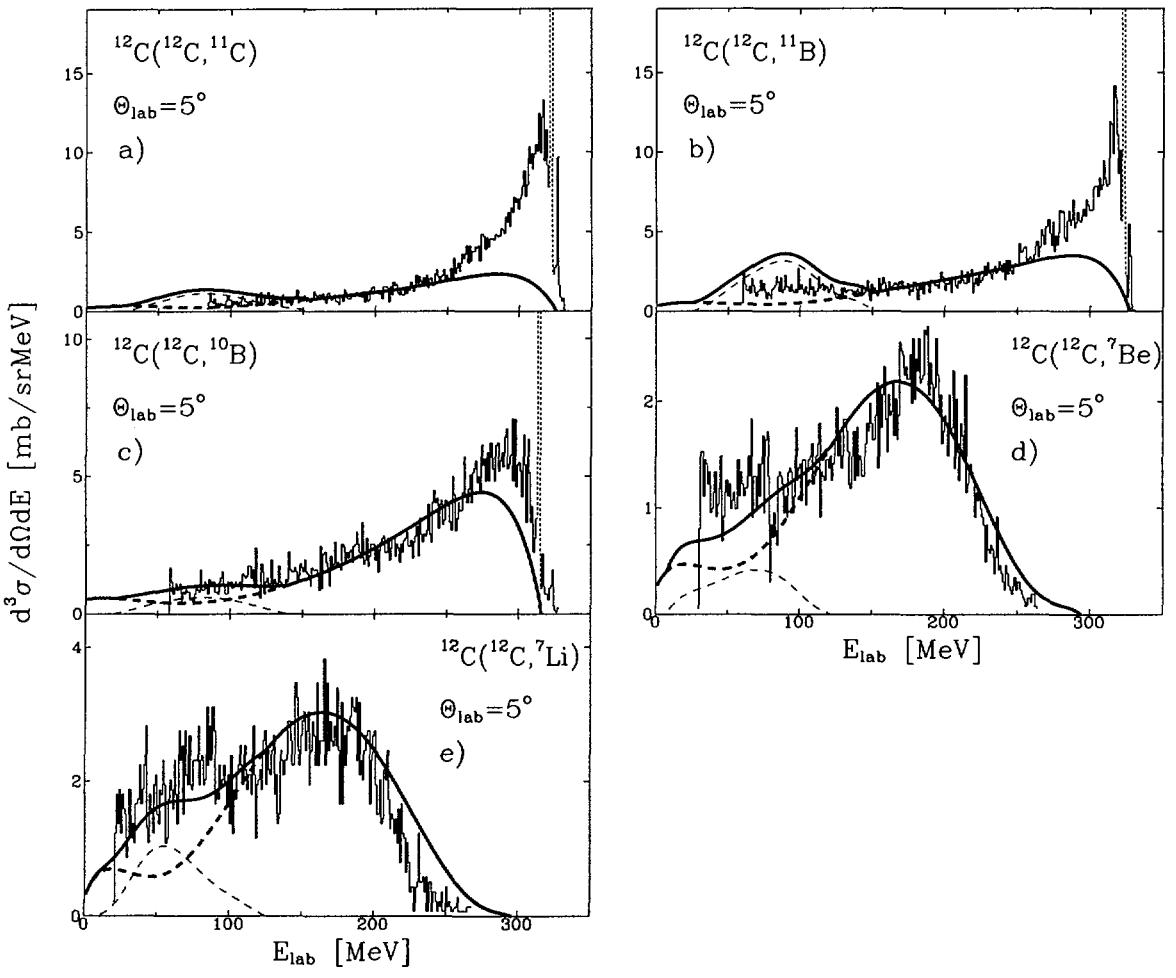

Fig. 41. Experimental inclusive spectra for laboratory angle $\theta_{lab}=5^o$ for ^{11}C, ^{11}B, ^{10}B, ^{7}Be and ^{7}Li ejectiles. Thick dashed lines represent the sum of the cross sections for corresponding sequential processes given in Table 1, thin dashed lines correspond to compound nucleus calculations and solid lines represent the sum of cross sections for these reactions.

Excited ^{12}C nucleus decays emitting α particle what leads to ^{8}Be nucleus decaying predominantly into two α particles. In the case of mutual projectile and target excitation above α particle decay threshold six α particles appear in the exit channel (Fig. 32). The calculations of α particle inclusive spectra as well as α–α coincidence spectra for such sequential process were performed. Since other processes contribute weakly this calculations should reproduce experimental α particle distributions. Therefore they were used to fix value of parameter $\gamma_{inel.}$. The shape of α particle inclusive spectra is sensitive to this parameters. It was found that inclusive α particle spectra at small laboratory angles are well reproduced using $\gamma_{inel.} = 0.03 - 0.05$ 1/MeV. The calculations of all sequential processes initiated by inelastic excitation were performed with $\gamma_{inel.} = 0.04$ 1/MeV. Such value of this parameter is confirmed by presented below analysis of ^{12}C spectra which is more restrictive. The α–α coincidence spectra contain information about excitation of intermediate ^{8}Be states, and can be used to determine relative strength of their occupation. In the analysis it was assumed that ^{8}Be nucleus is produced in ground state and first excited state only. As discussed in section 4.2 (see Fig. 32) the

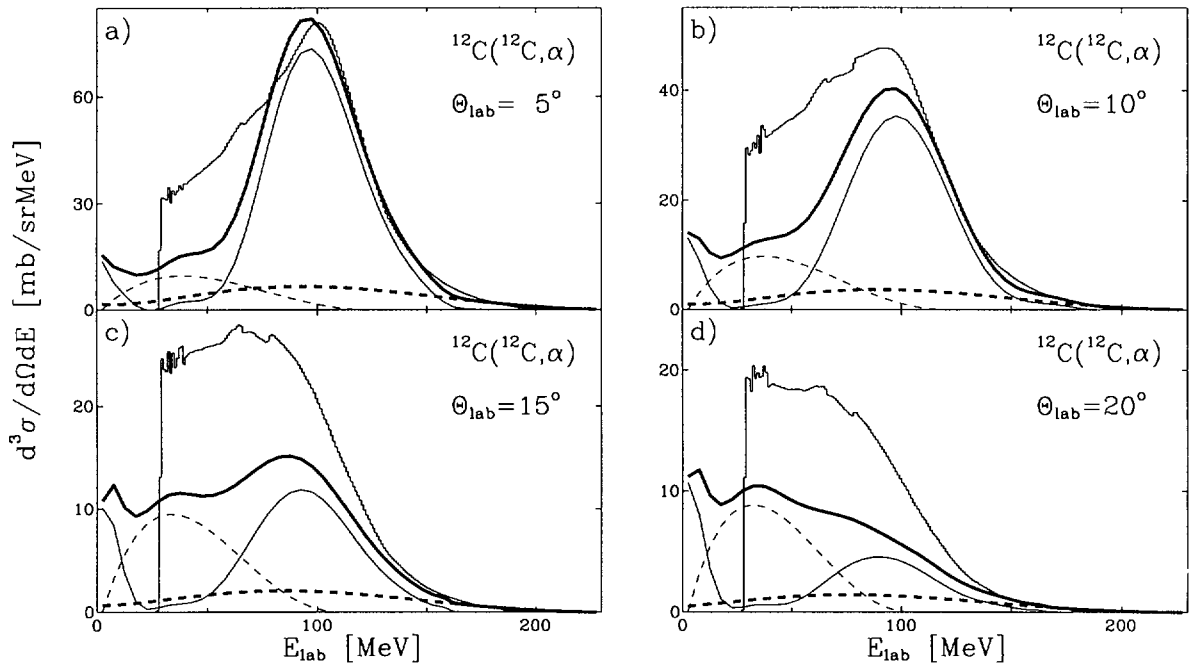

Fig. 42. Experimental inclusive α particle spectra compared with results of calculations for various processes. Thick dashed lines – sum of all sequential processes from Table 1 leading to α particle in the exit channel (except α+α+α channel), thin solid lines – sequential process leading to three or six α particles in the final state, thin dashed lines – α particles evaporated from compound nucleus and thick solid lines – sum of all these processes.

coincidences of α_1–α_2 particles from decay of ^{8}Be nucleus excited to 3.04 MeV state as well as coincidences of α_1–α_3 and α_2–α_3 particles for ^{8}Be in ground state and first excited state may be observed. The complex analysis of α particle spectra and α–α coincidences allows to determine the normalization factor N and relative strength of ^{8}Be nuclei production in ground and first excited states. From the comparison of the calculated and experimental α–α coincidence spectra for different angular configurations (presented in Fig. 43) it was found that ^{8}Be nuclei are produced in ground and first excited states with the same probability. The normalization factor N was adjusted in order to reproduce α–α coincidence cross section and α particle inclusive spectra were calculated with the same normalization factor. The results of the calculations performed for this sequential process are compared with experimental inclusive α particle spectra in Fig. 42 (thin solid line). It is seen that the contribution of this processes to experimental α particle cross section dominates. In Fig. 42 the sum of the cross section of all investigated sequential processes producing α particles and the cross section obtained for α particles evaporated from compound nucleus is also shown. It is visible that the reproduction of the experimental cross section for α particles by sum of cross sections for these processes is reasonable. Total cross section for ^{12}C decay into three α particles resulting from the analysis is given in Table 1.

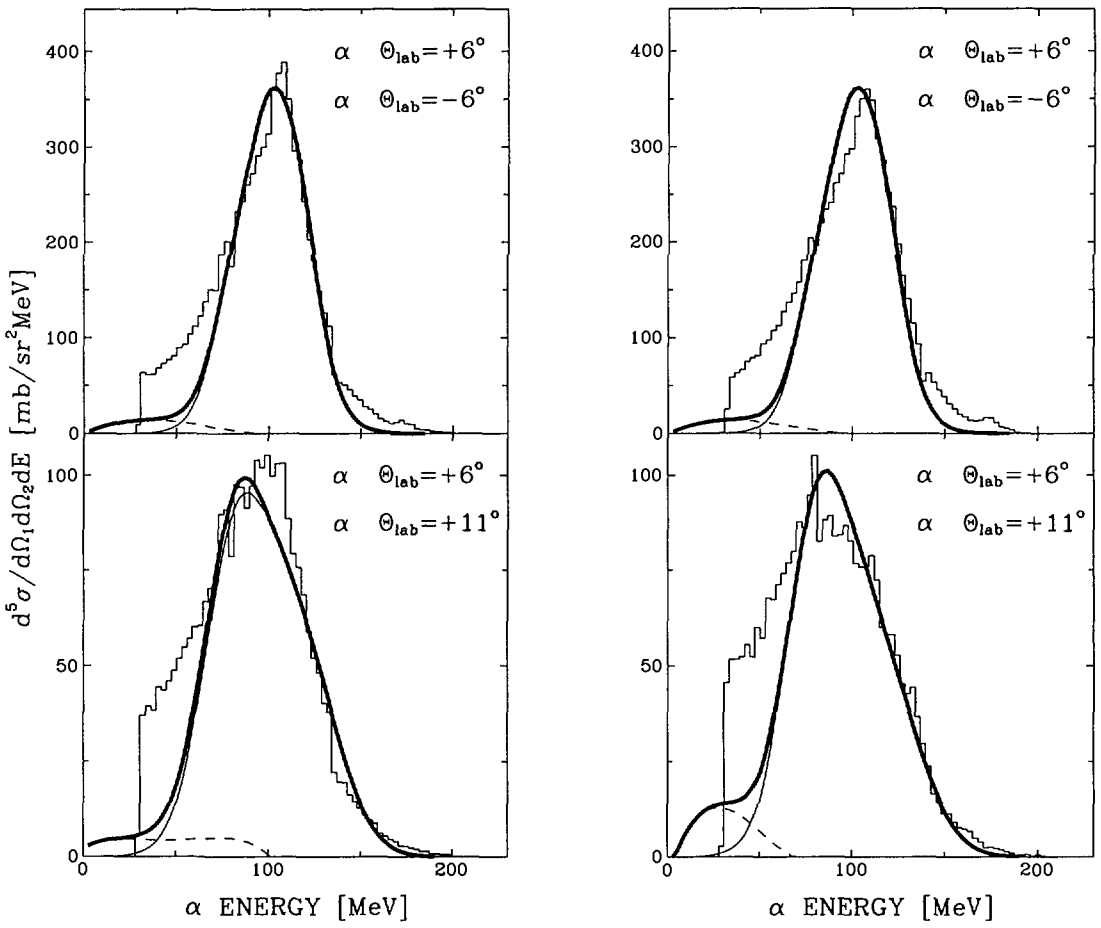

Fig. 43. Experimental α–α coincidence spectra compared with results of calculations for various processes. Thin solid lines – sequential process leading to three or six α particles in the final state, thin dashed lines – α particles evaporated from compound nucleus and thick solid lines – sum of these processes.

6.5. ^{12}C inclusive spectra

The distributions of ^{12}C ejectiles accompanying each regarded sequential process may be calculated with the same parameters as used in the analysis of these processes. Using fore–aft symmetry for identical particles in the entrance channel the calculated distributions may be compared with measured ^{12}C nuclei spectra. This is presented schematically in Fig. 44 for ^{12}C nucleus sequential decay into three α particles. In process (a) $^{12}C_1^*$ nucleus is excited above α particle decay threshold ($E_1^* > 7.4$ MeV) and decays into three α particles, while second $^{12}C_2^*$ nucleus may be in any energy state. The decay products – α particles are detected in the forward hemisphere. Using the symmetry for identical particles in the entrance channel, the same process is observed exchanging beam and target nuclei what is shown in Fig. 44b. In process (b) the $^{12}C_1^*$ nucleus is also excited to unbound states and decays into three α particles. Second $^{12}C_2^*$ nucleus may be excited to any energy, however in order to be detected it cannot be excited above decay threshold. While processes leading to α particles and $^{12}C_2^*$ ejectiles are identical, the only difference is that $^{12}C_2^*$ nucleus is detected only in bound states. The calculations of ^{12}C spectra for all sequential processes initiated by inelastic

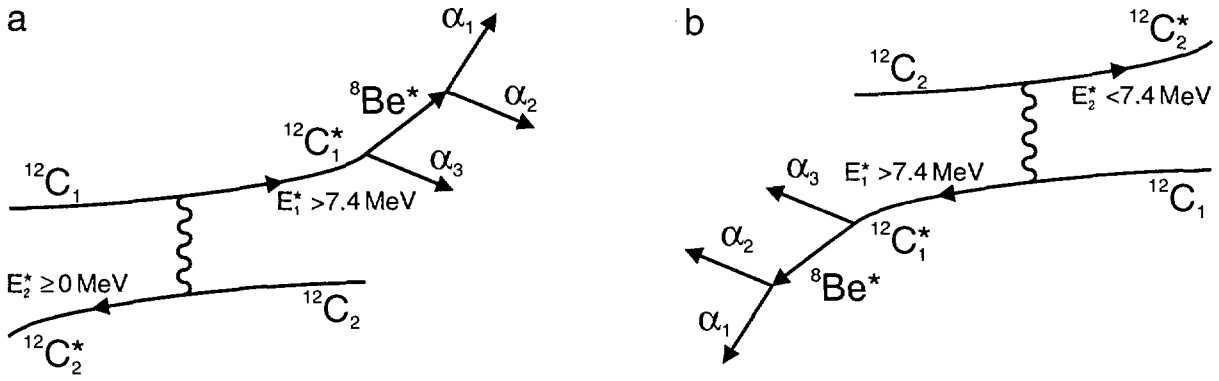

Fig. 44. Schematic representation of inelastic excitation followed by decay of projectile like $^{12}C_1^*$ nucleus with target like $^{12}C_2^*$ nucleus in any energy state (a). The same process observed by detection of target like $^{12}C_2^*$ nucleus excited to energy below decay threshold ($E_2^* < 7.4$ MeV) (b).

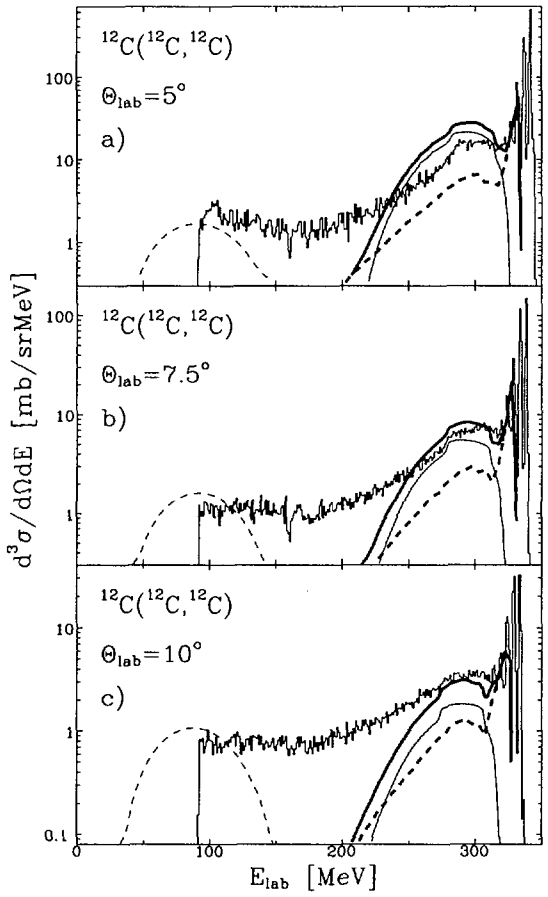

Fig. 45. Experimental ^{12}C inclusive spectra compared with the inelastic excitation cross section (thick dashed lines) derived from the sequential processes analysis using fore–aft symmetry of the cross section for identical particles in the entrance channel. Thin solid lines correspond to cross section for sequential processes initiated by nucleon transfer, thick solid lines – sum of these processes. Thin dashed lines correspond to compound nucleus calculations,

excitation (see Table 1) were performed with parameter $\gamma_{inel.} = 0.04$ 1/MeV. The analysis of ^{12}C distributions allows to determine value of this parameter more precisely. The calculated ^{12}C ejectiles cross section is too small or too large in comparison with experimental one for $\gamma_{inel.}$ parameter varied in the 0.03–0.05 1/MeV range. The normalization factors obtained from the analysis of each process were used, therefore ^{12}C cross section was calculated without free parameters. The sum of all these cross sections for ^{12}C production necessary for the description of various ejectiles distributions represents the whole inelastic excitation cross section. In Fig. 45 this cross section (thick dashed line) is compared with experimental data for ^{12}C nuclei. It is seen that the calculated inelastic excitation cross section may account for large portion of observed cross section, leaving however space for sequential processes initiated by nucleon transfer which were discussed in section 3.5 (thin solid line in Fig. 45). These processes are able to account for greater part of experimental cross section for ^{12}C ejectiles (thick solid line in Fig. 45). The cross section at low energies may be assigned to ^{12}C nuclei produced as evaporation residua (thin dashed line in Fig. 45).

6.6. Total cross sections for sequential processes

The relative importance of the various processes leading to various final nuclei is seen from Table 1. In the table the calculated total cross section for each regarded process is shown. From the analysis it was deduced that overall error of the obtained total cross section for each process is equal 15%. From Table 1 it is concluded that sequential processes initiated by inelastic excitation may account for about 800 mb cross section. In the inelastic excitation process both interacting nuclei are mutually excited to the energies larger than decay threshold. Using fore–aft symmetry appearing for identical particles in the entrance channel the values of parameters $\gamma_{inel.} = \zeta_{inel.}$ describing excitation probability of colliding nuclei were determined. Using these parameters it was deduced that mutual excitation above decay threshold account for about 75% of the inelastic excitation cross section. The sequential processes started by transfer give 200 mb, since to such processes listed in Table 1 also $^{13}C \rightarrow n+^{12}C$ and $^{13}N \rightarrow p+^{12}C$ sequential processes initiated by nucleon transfer (discussed in section 3.5) have to be added.

7. Conclusions

The reaction mechanism in $^{12}C+^{12}C$ system at intermediate energy of about 30 MeV/nucleon was studied. There are many controversies concerning processes leading to many particle final states at intermediate beam energies. Therefore, the system of two light colliding nuclei with small number of possible partitions in the exit channel was investigated. The contributions of various reaction mechanisms (inelastic scattering, transfer reactions, compound nucleus reactions, sequential decay following inelastic excitation and transfer) to the total reaction cross section were found. The analysis of inclusive and coincidence spectra allows to conclude that sequential fragmentation processes dominate. They are initiated by inelastic excitation or one and two nucleon transfer leading to unbound states with excitation energies well over the threshold for particle emission. These unbound states decay sequentially emitting various particles. It was shown that such fragmentation proceeds as one and two step sequential decay; in some cases even more steps decay was required in order to reproduce the experimental data. In the first stage of reaction both interacting nuclei may be excited in inelastic process to unbound state. Therefore, with large probability both colliding nuclei undergo sequential fragmentation.

These conclusions result from the analysis of the experimental data covering measurements of inclusive energy spectra in wide angular range and two particles coincidences for various angular configurations. Very good separation of ejectiles with different charge and mass as well as low detection threshold achieved in the measurements were very important in the performed analysis. The fore–aft symmetry of the cross section in the center of mass system, resulting from the particle identity in the entrance channel, was used as the strong test of the consistency of the performed analysis.

The model independent analysis of the experimental coincidence spectra allowed to conclude that sequential decay processes play most important role. In case of all measured coincidences the excitation of intermediate nuclei was observed. The observation of excitation of intermediate nuclei states, practically without continuous background, allows to deduce the dominating sequence of the decay and suggests that prompt fragmentation may be in most cases excluded. Only in case of α–α coincidences the occurrence of the prompt fragmentation of ^{12}C nuclei into three α particles could not be excluded. However, it should have quite small cross section since the experimental data are well described without considering such process.

Quantitative results concerning the probability of various sequential fragmentation processes were obtained from the phenomenological model. It was shown that sequential fragmentation processes very well describe the shape of energy and angular distributions of inclusive cross sections in the whole measured energy and angular range. Also the most important features of the experimental coincidence cross section for all measured angular configurations may be reproduced by calculated sequential processes. The normalization factors obtained from the analysis were used to determine the cross section for each regarded fragmentation process.

Very good description of experimental data obtained in quantitative analysis allows to make an effort to accomplish balance of the total reaction cross section. The obtained total inelastic excitation

cross section followed by the decay was found to be 800 mb, and that of the transfer reactions followed by the decay is 200 mb. Therefore the total cross section for the sequential fragmentation processes was estimated to be 1000 mb. The calculated cross section for compound nucleus reaction was found to be 200 mb. The experimental cross section corresponding to two body processes (integrated cross section for measured discrete state transitions) equals to about 40 mb. All these processes give in total 1240 mb cross section with an estimated error ±200 mb what agrees very well with total reaction cross section of 1290 mb obtained from the optical model calculations. Thus the sequential processes may account for about 80% of the total reaction cross section, fusion for about 15% and rest of 5% have to be attributed to the direct processes with ejectiles being in bound states.

The results of performed studies allow to conclude that investigations of similar systems of colliding nuclei at various energies would enable to find the evolution of the reaction mechanisms from low to high energy region. The development of reaction mechanism from fusion dominated region at low energies (50–90% of the total reaction cross section) to prevailing sequential fragmentation at intermediate energy is already visible from the presented analysis. Searching for the new reaction mechanism, the sequential processes have to be carefully analysed, since they contribute with large cross section in the whole energy and angular range of outgoing particles.

References

1. L. G. Moretto, G. J. Wozniak, Ann. Rev. Nucl. Part. Sci. **43** (1993) 379;
   H. Fuchs, K. Möhring, Rep. Prog. Phys. **57** (1994) 231.
2. J. Péter, S. C. Jeong, J. C. Angélique, G. Auger, G. Bizard, R. Brou, A. Buta, C. Cabot, Y. Cassagnou, E. Crema, D. Cussol, D. Durand, Y. El Masri, P. Eudes, Z. Y. He, A. Kerambrun, C. Lebrun, R. Legrain, J. P. Patry, A. Péghaire, R. Régimbart, E. Rosato, F. Saint–Laurent, J. C. Steckmeyer, B. Tamain, E. Vient, Nucl. Phys. **A593** (1995) 95.
3. F. Saint–Laurent, Nucl. Phys. **A583** (1995) 481.
4. M. Samri, G. C. Ball, L. Beaulieu, B. Djerroud, D. Doré, Galindo–Uribarri, P. Gendron, E. Hagberg, D. Horn, E. Jalbert, R. Laforest, Y. Larochelle, J. Pouliot, R. Roy, C. St.–Pierre, Nucl. Phys. **A583** (1995) 427.
5. A. Siwek, A. Sourell, A. Budzanowski, H. Fuchs, H. Homeyer, G. Pausch, W. Kantor, G. Röschert, C. Schwarz, W. Terlau, A. Tutay, Z. Phys. **A350** (1995) 327.
6. L. Beaulieu, R. Laforest, J. Pouliot, R. Roy, C. St–Pierre, G. C. Ball, E. Hagberg, D. Horn, R. B. Walker, Nucl. Phys. **A580** (1994) 81.
7. P. F. Box, K. A. Griffioen, P. Decowski, T. Bootsma, E. Gerlik, G. J. van Nieuwenhuizen, C. Twenhöfel, R. Kamermans, H. W. Wilschut, A. Giorni, C. Morand, A. Demeyer, D. Guinet, Phys. Rev. **C50** (1994) 934.
8. K. Hagel, M. Gonin, R. Wada, J. B. Natowitz, F. Haddad, Y. Lou, M. Gui, D. Utley, B. Xiaó, J. Li, G. Nebbia, D. Fabris, G. Prete, J. Ruiz, D. Drain, B. Cheynis, D. Duinet, X. C. Hu, A. Demeyer, C. Pastor, A. Giorni, A. Lleres, P. Stassi, J. B. Viano, P. Gonthier, Phys. Rev. **C50** (1994) 2017.
9. D. Heuer, A. Chabane, M. E. Brandan, M. Charvet, A. J. Cole, P. Désesquelles, A. Giorni, A. Lleres, A. Menchaca–Rocha, J. B. Viano, D. Benchekroun, B. Cheynis, A. Demeyer, E. Gerlic, D. Guinet, M. Stern, L. Vagneron, Phys. Rev. **C50** (1994) 1943.
10. R. Laforest, D. Doré, J. Pouliot, R. Roy, G. Auger, P. Bricault, S. Groult, E. Plagnol, D. Horn, Nucl. Phys. **A568** (1994) 350.
11. A. Lleres, A. J. Cole, P. Désesquelles, A. Giorni, D. Heuer, J. B. Viano, B. Chambon, B. Cheynis, D. Drain, C. Pastor, Phys. Rev. **C50** (1994) 1973.
12. F. Andreozzi, A. Brondi, A. D'Onofrio, G. LaRana, R. Moro, E. Perillo, M. Romano, F. Terrasi, R. Dayras, H. Dumont, F. Gadi, J. Gomez del Campo, Nucl. Phys. **A564** (1993) 441.
13. A. Badalà, R. Barbera, A. Palmeri, G. S. Pappalardo and F. Riggi, Phys. Rev. **C48** (1993) 633.
14. E. Bauge, A. Elmaani, Roy A. Lacey, N. N. Ajitanand, D. Craig, M. Cronqvist, E. Gualtieri, S. Hannuschke, T. Li, B. Llope, T. Reposeur, A. Vander Molen, G. D. Westfall, J. S. Winfield, J. Yee, S. Yennello, A. Nadasen, R. S. Tickle, E. Norbeck, Phys. Rev. Lett. **70** (1993) 3705.
15. E. Chavez-Lomeli, A. Dacal, M. E. Ortiz, S. B. Gazes, Y. Chan, R. G. Stokstad, E. Plagnol, K. Siwek-Wilczynska, J. Wilczynski, Phys. Rev. **C48** (1993) 699.

16. D. Cussol, G. Bizard, R. Brou, D. Durand, M. Louvel, J. P. Patry, J. Péter, R. Ragimbart, J. C. Steckmeyer, J. P. Sullivan, B. Tamain, E. Crema, H. Doubre, K. Hagel, G. M. Jin, A. Péghaire, F. Saint–Laurent, Y. Cassagnou, R. Legrain, C. Lebrun, E. Rosato, R. MacGrath, S. C. Jeong, S. M. Lee, Y. Nagashima, T. Nakagawa, M. Ogihara, J. Kasagi, T. Motobayashi, Nucl. Phys. **A561** (1993) 298.
17. P. Désesquelles, A. J. Cole, A. Giorni, D. Heuer, A. Lleres, J. B. Viano, B. Chambon, B. Cheynis, D. Drain, C. Pastor, Phys. Rev. **C48** (1993) 1828.
18. T. Ethvignot, J. M. Alexander, A. J. Cole, A. Elmaani, P. Désesquelles, H. Elhage, A. Giorni, D. Heuer, S. Kox, A. Lleres, F. Merchez, C. Morand, D. Rebreyend, P. Stassi, J. B. Viano, F. Benrachi, B. Chambon, B. Cheynis, D. Drain, C. Pastor, Phys. Rev. **C48** (1993) 618.
19. T. Li, W. Bauer, D. Craig, M. Cronqvist, E. Gualtieri, S. Hannuschke, R. Lacey, W. L. Llope, T. Reposeur, A. M. Vander Molen, G. G. Westfall, W. K. Wilson, J. S. Winfield, J. Yee, S. J. Yennello, A. Nadasen, R. S. Tickle, E. Norback, Phys. Rev. Lett. **70** (1993) 1924.
20. A. Lleres, A. Giorni, H. Elhage, M. E. Brandan, A. J. Cole, P. Désequelles, D. Heuer, A. Menchaca–Rocha, J. B. Viano, F. Benrachi, B. Chambon, B. Cheynis, D. Drain, C. Pastor, Phys. Rev. **C48** (1993) 2753.
21. M. Louvel, T. Hamdani, G. Bizard, R. Bougault, R. Brou, H. Doubre, D. Durand, Y. El Masri, H. Fugiwara, A. Genoux–Lubain, K. Hagel, A. Hajfani, F. Hanappe, S. C. Jeong, G. M. Jin, S. Kato, J. L. Laville, C. Le Brun, J. F. Lecolley, S. Lee, T. Matsuse, T. Motobayashi, J. P. Patry, A. Péghaire, J. Péter, N. Prot, R. Regimbart, F. Saint–Laurent, J. C. Steckmeyer, B. Tamain, Nucl. Phys. **A559** (1993) 137.
22. W. Q. Shen, J. Péter, G. Bizard, R. Brou, D. Cussol, M. Louvel, J. P. Patry, R. Régimbart, J. C. Steckmeyer, J. P. Sullivan, B. Tamain, E. Crema, H. Doubre, K. Hagel, G. M. Jin, A. Péghaire, F. Saint–Laurent, Y. Cassagnou, R. Legrain, C. Lebrun, E. Rosato, R. MacGrath, S. C. Jeong, S. M. Lee, Y. Nagashima, T. Nakagawa, M. Ogihara, J. Kasagi, T. Motobayashi, Nucl. Phys. **A551** (1993) 333.
23. A. Sokolov, D. Guerreau, J. L. Charvet, B. Cramer, H. Doubre, J. Fréhaut, J. Galin, B. Gatty, G. Inglod, D. Jacquet, U. Jahnke, D. X. Jiang, B. Lott, C. Magnago, M. Morjean, Y. Patin, E. Piasecki, J. Pouthas, E. Schwinn, Nucl. Phys. **A562** (1993) 273.
24. M. Stern, E. Gerlic, R. Billerey, B. Chambon, A. Chevarier, N. Chevarier, B. Cheynis, D. Drain, C. Pastor, C. Vincent-Donnet, A. Giorni, D. Heuer, A. Lleres, J. B. Viano, P. L. Gonthier, Nucl. Phys. **A559** (1993) 401.
25. P. Decowski, E. Gierlik, P. F. Box, K. A. Griffioen, R. J. Meijer, G. J. van Nieuwenhuizen, R. Kamermans, H. W. Wilschut, A. Giorni, C. Morand, A. Demeyer, D. Guinet, Phys. Rev. **C46** (1992) 667.
26. D. Doré, L. Beaulieu, R. Laforest, J. Pouliot, R. Roy, C. St–Pierre, G. Auger, P. Bricault, S. Groult, E. Plagnol, S. Groult, Nucl. Phys. **A545** (1992) 363c.
27. K. Hagel, M. Gonin, R. Wada, J. B. Natowitz, B. H. Sa, Y. Lou, M. Gui, D. Utley, G. Nebbia, D. Fabris, G. Prete, J. Ruiz, D. Drain, B. Chambon, B. Cheynis, D. Guinet, X. C. Hu,

A. Demeyer, C. Pastor, A. Giorni, A. Lleres, P. Stassi, J. B. Viano, P. Gonthier, Phys. Rev. Lett. **68** (1992) 2141.

28. Y. D. Kim, R. T. de Souza, D. R. Bowman, N. Carlin, C. K. Gelbke, W. G. Gong, W. G. Lynch, L. Phair, M. B. Tsang, F. Zhu, Phys. Rev. **C45** (1992) 338.
29. L. Phair, D. R. Bowman, C. K. Gelbke, W. G. Gong, Y. D. Kim, M. A. Lisa, W. G. Lynch, G. F. Peaslee, R. T. de Souza, M. B. Tsang, F. Zhu, Nucl. Phys. **A548** (1992) 489.
30. J. L. Wille, D. E. Fields, K. Kwiatkowski, S. J. Yennello, K. B. Morley, E. Renshaw, V. E. Viola, C. K. Gelbke, W. G. Lynch, N. Carlin, H. M. Xu, W. G. Gong, M. B. Tsang, J. Pochodzalla, R. T. de Souza, D. J. Fields, Sam M. Austin, Phys. Rev. **C45** (1992) 2300.
31. D. R. Bowman, G. F. Peaslee, N. Colonna, R. J. Charity, M. A. McMahan, D. Delis, H. Han, K. Jing, G. J. Wozniak, L. G. Moretto, W. L. Kehoe, B. Libby, A. C. Mignerey, A. Moroni, S. Angius, I. Iori, A. Pantaleo, G. Guarino, Nucl. Phys. **A523** (1991) 386.
32. J. Pouliot, Y. Chan, D. E. DiGregorio, B. A. Harmon, R. Knop, C. Moisan, R. Roy, R. G. Stokstad, Phys. Rev. **C43** (1991) 735.
33. D. A. Cebra, S. Howden, J. Karn, A. Nadasen, C. A. Ogilvie, A. Vander Molen, G. D. Westfall, W. K. Wilson, J. S. Winfield, E. Norbeck, Phys. Rev. Lett. **64** (1990) 2246.
34. M. C. Etchegoyen, A. Etchegoyen, A. O. Macchiavelli, G. Crawley, C. Dajali, M. Rentería, A. Szanto de Toledo, G. Westfall, Nucl. Phys. **A518** (1990) 572.
35. P. L. Gonthier, P. Harper, B. Bouma, R. Ramaker, D. A. Cebra, Z. M. Koenig, D. Fox, G. D. Westfall, Phys. Rev. **C41** (1990) 2635.
36. B. A. Harmon, J. Pouliot, J. A. López, J. Suro, R. Knop, Y. Chan, D. E. DiGregorio, R. G. Stokstad, Phys. Lett. **B235** (1990) 234.
37. B. Jakobsson, G. Jönsson, L. Karlsson, V. Kopljar, B. Norén, K. Söderström, F. Schussler, E. Monnand, H. Nifenecker, G. Fai, J. P. Bondorf, K. Sneppen, Nucl. Phys. **A509** (1990) 195.
38. M. Westenius, M. Berg, H.–Å. Gustafsson, B. Jakobsson, A. Kristiansson, A. Oskarsson, H. Ryde, S. Kox, F. Merchez, F. Schussler, J. P. Bondorf, O.–B. Nielsen, E. Andersen, G. Løvhøiden, T. F. Thorsteinsen, M. Maurel, Nucl. Phys. **A509** (1990) 630.
39. A. Kiss, F. Deák, Z. Seres, G. Caskey, A. Galonsky, B. Remington, L. Heilbronn, Nucl. Phys. **A499** (1989) 131.
40. D. Pelte, U. Winkler, M. Gnirs, A. Gobbi, K. D. Hildenbrand, R. Novotny, Phys. Rev. **C39** (1989) 553.
41. C. Pruneau, L. Potvin, R. Roy, C. St-Pierre, G. C. Ball, R. Bougault, E. Hagberg, D. Horn, D. Cebra, D. Fox, G. D. Westfall, Nucl. Phys. **A500** (1989) 168.
42. J. Richert, P. Wagner, Z. Phys. **A330** (1988) 283.
43. M. Stern, R. Billerey, B. Chambon, A. Chbihi, A. Chevarier, N. Chevarier, B. Cheynis, D. Drain, C. Pastor, J. Alarja, A. Dauchy, A. Giorni, D. Heuer, C. Morand, J. B. Viano, Z. Phys. **A331** (1988) 323.
44. W. Terlau, M. Bürgel, A. Budzanowski, H. Fuchs, H. Homeyer, G. Röschert, J. Uckert, R. Vogel, Z. Phys. **A330** (1988) 303.

45. Z. Chen, C. K. Gelbke, W. G. Gong, Y. D. Kim, W. G. Lynch, M. R. Maier, J. Pochodzalla, M. B. Tsang, F. Saint-Laurent, D. Ardouin, H. Delagrange, H. Ardouin, H. Delagrange, H. Doubre, J. Kasagi, A. Kyanowski, A. Péghaire, J. Péter, E. Rosato, G. Bizard, F. Lefèbvres, B. Tamain, J. Québert, Y. P. Viyogi, Phys. Rev. **C36** (1987) 2297.
46. P. L. Gonthier, B. Bouma, P. Harper, R. Ramaker, D. A. Cebra, Z. M. Koenig, D. Fox, G. D. Westfall, Phys. Rev. **C35** (1987) 1946.
47. B. V. Jacak, G. D. Westfall, G. M. Crawley, D. Fox, C. K. Gelbke, W. G. Lynch, D. K. Scott, H. Stöcker, M. B. Tsang, G. Buchwald, T. J. M. Symons, Phys. Rev. **C35** (1987) 1751.
48. G. S. F. Stephans, R. V. F. Janssens, D. G. Kovar, B. D. Wilkins, Phys. Rev. **C35** (1987) 614.
49. R. Ost, A. Gamp, S. Kox, C. Perrin, N. Longequeue, F. Merchez, Phys. Rev. **C32** (1985) 1927.
50. M. Begemann-Blaich, W. F. J. Müller, J. Aichelin, J. C. Adloff, P. Bouissou, J. Hubele, G. Imme, I. Iori, P. Kreutz, G. J. Kunde, S. Leray, V. Lindenstruth, Z. Liu, U. Lynen, R. J. Meijer, U. Milkau, A. Moroni, C. Ngô, C. A. Oglivie, J. Pochodzalla, G. Raciti, G. Rudolf, H. Sann, A. Schüttauf, W. Seidel, L. Stuttge, W. Trautmann, A. Tucholski, Phys. Rev. **C48** (1993) 610.
51. W. A. Friedman, Phys. Rev. **C42** (1990) 667.
52. D. H. E. Gross, Rep. Prog. Phys. **53** (1990) 605.
53. J. A. López, J. Randrup, Nucl. Phys. **A512** (1990) 345.
54. J. A. López, J. Randrup, Nucl. Phys. **A503** (1989) 183.
55. R. J. Charity, M. A. McMahan, G. L. Wozniak, R. J. McDonald, L. G. Moretto, D. G. Sarantites, L. G. Sobotka, G. Guarino, A. Panateleo, L. Fiore, A. Gobbi, K. D. Hildenbrand, Nucl. Phys **A483** (1988) 371.
56. W. A. Friedman, Phys. Rev. Lett. **60** (1988) 2125.
57. J. P. Bondorf, R. Donangelo, I. N. Mishustin, C. J. Pethick, H. Schulz, K. Sneppen, Nucl. Phys. **A443** (1987) 321.
58. D. H. E. Gross, H. Massmann, Nucl. Phys. **A471** (1987) 339c.
59. C. J. Pethick, D. G. Ravenhall, Nucl. Phys. **A471** (1987) 19c.
60. H. W. Barz, J. P. Bondorf, R. Donangelo, H. Schulz, Phys. Lett. **B169** (1986) 318.
61. G. Bertsch, P. J. Siemens, Phys. Lett. **B126** (1983) 9.
62. W. A. Friedman, W. G. Lynch, Phys. Rev. **C28** (1983) 16.
63. J. Czudek, L. Jarczyk, B. Kamys, A. Magiera, R. Siudak, A. Strzałkowski, B. Styczeń, J. Hebenstreit, W. Oelert, P. von Rossen, H. Seyfarth, A. Budzanowski, A. Szczurek, Phys. Rev. **C43** (1991) 1248.
64. Z. Seres, F. Deák, A. Kiss, G. Caskey, A. Galonsky, L. Heilbronn, B. Remington, Nucl. Phys. **A492** (1989) 315.
65. A. J. Cole, Z. Phys. **A322** (1985) 315.
66. A. J. Cole, R. Cherkaoui-Tadili, J. Alarja, Phys. Rev. **C40** (1989) 1265.
67. K. W. McVoy, M. Carolina Nemes, Z. Phys. **A295** (1980) 177.
68. H. Utsunomiya, Phys. Rev. **C32** (1985) 849.
69. J. A. López, J. Randrup, Nucl. Phys. **A491** (1989) 477.

70. S. J. Yenello, K. Kwiatkowski, E. C. Pollacco, C. Volant, Y. Cassagnou, R. Dayras, D. E. Fields, S. Harar, E. Hourani, R. Legrain, E. Norbeck, R. Płaneta, J. L. Wile, N. R. Yoder, V. E. Viola, Phys. Rev. **C48** (1993) 1092.
71. W. Gawlikowicz, K. Grotowski, Nucl. Phys. **A551** (1993) 73.
72. P. Pawłowski, J. Brzychczyk, D. Benchekrovn, E. Bisquer, P. Burzyński, A. Chabane, M. Charvet, B. Cheynis, A. J. Cole, A. Demeyer, P. Désesquelles, W. Gawlikowicz, E. Gerlic, A. Giorni, K. Grotowski, D. Guinet, P. Hachaj, D. Heuer, P. Lautesse, L. Lebreton, A. Lleres, S. Micek, R. Płaneta, Z. Sosin, M. Stern, L. Vagneron, B. Viano, A. Wieloch, Phys. Rev. **C54** (1996) in press.
73. K. Hagel, A. Péghaire, G. M. Jin, D. Cussol, H. Doubre, J. Péter, F. Saint–Laurent, G. Bizard, R. Brou, M. Louvel, J. P. Patry, R. Regimbart, J. C. Steckmeyer, B. Tamain, Y. Cassagnou, R. Legrain, C. Lebrun, E. Rosato, R. Mac Grath, S. C. Jeong, S. M. Lee, Y. Nagashima, T. Nakagawa, M. Ogihara, J. Kasagi, T. Motobayashi, Phys. Lett. **B229** (1989) 20.
74. L. Jarczyk, B. Kamys, A. Magiera, R. Siudak, A. Strzałkowski, B. Styczeń, J. Hebenstreit, W. Oelert, P. von Rossen, H. Seyfarth, G.R. Satchler, Nucl. Phys. **A518** (1990) 583.
75. L. Jarczyk, B. Kamys, A. Magiera, Z. Rudy, A. Strzałkowski, B. Styczeń, J. Hebenstreit, W. Oelert, P. von Rossen, H. Seyfarth, Z. Phys. **A342** (1992) 169.
76. R. Siudak, Ph. D. thesis, Jagellonian University, Cracow, 1993.
77. H. Lenske, R. Siudak, H.H. Wolter, L. Jarczyk, B. Kamys, A. Magiera, A. Strzałkowski, B. Styczeń, J. Hebenstreit, W. Oelert, P. von Rossen, H. Seyfarth, to be publish.
78. F. S. Goulding, in Treatise on Heavy Ion Science, edited by D. A. Bromley (Plenum, New York), vol. 7, p. 235.
79. C. Beck, F. Haas, R. M. Freeman, B. Heusch, J. P. Coffin, G. Guillaume, F. Rami, P. Wagner, Nucl. Phys. **A442** (1985) 320.
80. J. Gomez del Campo, J. A. Biggerstaff, R. A. Dayras, D. Shapira, A. H. Snell, P. H. Stelson, R. G. Stokstad, Phys. Rev. **C29** (1984) 1722.
81. D. E. DiGregorio, J. Gomez del Campo, Y. D. Chan, J. L. C. Ford, Jr., D. Shapira, M. E. Oritz, Phys. Rev. **C26** (1982) 1490.
82. J. Gomez del Campo, R. G. Stokstad, J. A. Biggerstaff, R. A. Dayras, A. H. Snell, P. H. Stelson, Phys. Rev. **C19** (1979) 2170.
83. A. Gavron, in Computational Nuclear Physics 2, edited by K. Langanke, J.A. Maruhn, S.E. Koonin (Springer–Verlag, New York, 1993), p.108.
84. A. Gilbert, A.G.W. Cameron, Can. J. Phys. **43** (1965) 1446.
85. T.D. Newton, Can. J. Phys. **34** (1956) 804.
86. L. Jarczyk, B. Kamys, J. Okołowicz, J. Sromicki, A. Strzałkowski, H. Witała, Z. Wróbel, M. Hugi, J. Lang, R. Müller, E. Ungricht, Nucl. Phys. **A325** (1979) 510.
87. M. Kistryn, L. Jarczyk, B. Kamys, A. Magiera, Z. Rudy, A. Strzałkowski, R. Barná, V. D'Amico, D. De Pasquale, A. Italiano, M. Licandro, to be published in Phys. Rev. C.
88. M. Kistryn, Ph.D. thesis, Jagellonian University, Cracow 1996.

89. L. C. Vaz, J. M. Alexander, G. R. Satchler, Phys. Rep. **69** (1981) 373.
90. L. Jarczyk, B. Kamys, A. Magiera, J. Sromicki, A. Strzałkowski, G. Willim, Z. Wróbel, D. Balzer, K. Bodek, M. Hugi, J. Lang, R. Müller, E. Ungricht, Nucl. Phys. **A369** (1981) 191.
91. F. Porto, S. Sambataro, Nuovo Cimento **83A** (1984) 339.
92. S. Cohen, F. Plasil, W. J. Swiatecki, Ann. Phys. **82** (1974) 557.
93. D. M. Brink, Phys. Lett. **B40** (1972) 37.
94. N. Anyas–Weiss, J. C. Cornell, P. S. Fisher, P. N. Hudson, A. Menchaca–Rocha, D. J. Millener, A. D. Panagiotou, D. K. Scott, D. Strottman, D. M. Brink, B. Buck, P. J. Ellis, T. Engeland, Phys. Rep. **12C** (1974) 201.
95. J. Hebenstreit, Ph.D. Thesis, Jagellonian University, Cracow 1996.
96. T. Tamura, T. Udagawa, H. Lenske, Phys. Rev. **C26** (1981) 379.
97. P. von Neumann–Cosel, A. Richter, H.–J. Schmidt–Brücken, G. Schrieder, H. Lenske, H. H. Wolter, J. Carter, R. Jahn, B. Kohlmeyer, D. Schüll, Nucl. Phys. **A516** (1990) 385.
98. F. J. Eckle, H. Lenske, G. Eckle, G. Graw, R. Hertenberger, H. Kader, F. Merz, H. Nann, P. Schiemenz, H. H. Wolter, Phys. Rev. **C39** (1989) 1662.
99. F. J. Eckle, H. Lenske, G. Eckle, G. Graw, R. Hertenberger, H. Kader, H. J. Maier, F. Merz, H. Nann, P. Schiemenz, H. H. Wolter, Nucl. Phys. **A506** (1990) 159.
100. A. Szczurek, A. Budzanowski, L. Jarczyk, A. Magiera, K. Möhring, R. Siudak, T. Srokowski, Z. Phys. **A338** (1991) 187.

Acknowledgements

I am very grateful to Professor L. Jarczyk and Professor A. Strzałkowski for their continued interest and for many valuable discussions.

I owe Professor O.W.B. Schult a debt of gratitude for the possibility to perform experiments in Kernforschungszentrum KFA Jülich.

I am very indebted to my colleagues W. Oelert, P. von Rossen and H. Seyfarth from Kernforschungszentrum KFA Jülich for their help in preparations and running the experiments.

I would like to thank my colleagues from the Jagellonian University for their incessant help and especially to Dr J. Hebenstreit for assistance in the experiments and Dr B. Styczeń for help in the data evaluation.

Andrzej Magiera